SC71056.FR

Copy No. 3

A Study of the Use of β-Alumina as a Weak Interface in Alumina Fiber Composites

FINAL REPORT

CONTRACT NO. N00014-91-C-0157

Prepared for:

Dr. S. Fishman
Program Manager Non-Metallic Materials
Office of Naval Research
800 N. Quincy St.
Arlington, VA 22217-5000

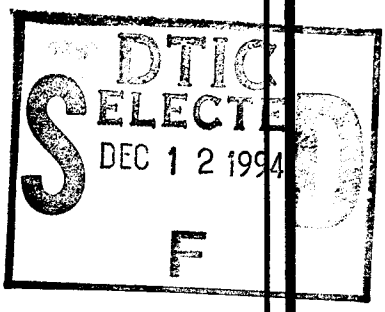

D.B. Marshall and P.E.D. Morgan
Principal Investigators

November 1994

Approved for public release; distribution unlimited

Rockwell International
Science Center

The Contractor, Rockwell International Corporation Science Center, hereby certifies that, to the best of its knowledge and belief, the technical data delivered herewith under Contract No. N00014-91-C-0157 is complete, accurate, and complies with all requirements of the contract.

D. B. Marshall

November 16, 1994
Date

D. B. Marshall, Manager, Structural Ceramics
Name and Title of Certifying Official

REPORT DOCUMENTATION PAGE

Form Approved
OMB No. 0704-0188

1. AGENCY USE ONLY *(Leave Blank)*	2. REPORT DATE	3. REPORT TYPE AND DATES COVERED
	November 1994	Final 09-01-91 through 08-31-94

4. TITLE AND SUBTITLE

A STUDY OF THE USE OF β-ALUMINA AS A WEAK INTERFACE IN ALUMINA FIBER COMPOSITES

5. FUNDING NUMBERS

4. AUTHOR(S)

D.B. Marshall and P.E.D. Morgan

7. PERFORMING ORGANIZATION NAME(S) AND ADDRESS(ES)

Rockwell International Science Center
P.O. Box 1085
Thousand Oaks, CA 91358

7. PERFORMING ORGANIZATION REPORT NUMBER

SC71056.FR

9. SPONSORING / MONITORING AGENCY NAME(S) AND ADDRESS(ES)

Dr. S. Fishman
Program Manager Non-Metallic Materials
Office of Naval Research
800 N. Quincy St.
Arlington, VA 22217-5000

9. SPONSORING / MONITORING AGENCY REPORT NUMBER

11. SUPPLEMENTARY NOTES

12a. DISTRIBUTING/AVAILABILITY STATEMENT

12b. DISTRIBUTION CODE

13. ABSTRACT *(Maximum 200 Words)*

Results are presented from a three–year study aimed at identifying and developing suitable interphase materials for oxide-oxide composites that are stable in high temperature oxidizing environments, yet sufficiently weak to allow debonding as required for toughening. Most of the effort was devoted to two systems: $LaPO_4$ (monazite) and β-aluminas. Monazite satisfied all of the requirements for an interphase in alumina–alumina composites (and most likely many other ceramic matrix-fiber combinations). It has a high melting point (2074°C); it is stable with alumina at high temperature in both oxidizing and slightly reducing environments ; and it forms a sufficiently weak bond with alumina. β-alumina materials, which possess weak mica-like planes in their crystal structures, are phase-compatible with alumina, and their debonding characteristics are adequate. However, their use and fabrication temperatures are limited by morphological instability of the fiber/matrix interface (grain growth of the β-alumina platelets into the fibers).

14. SUBJECT TERMS	15. NUMBER OF PAGES
Monazite, β-alumina	**97**
	16. PRICE CODE

17. SECURITY CLASSIFICATION OF REPORT	18. SECURITY CLASSIFICATION OF THIS PAGE	19. SECURITY CLASSIFICATION OF ABSTRACT	20. LIMITATION OF ABSTRACT
Unclassified	**Unclassified**	**Unclassified**	

Table of Contents

Abstract

Results are presented from a three–year study aimed at identifying and developing suitable interphase materials for oxide-oxide composites that are stable in high temperature oxidizing environments, yet sufficiently weak to allow debonding as required for toughening. Most of the effort was devoted to two systems: $LaPO_4$ (monazite) and β-aluminas. Monazite satisfied all of the requirements for an interphase in alumina–alumina composites (and most likely many other ceramic matrix-fiber combinations). It has a high melting point (2074°C); it is stable with alumina at high temperature in both oxidizing and slightly reducing environments ; and it forms a sufficiently weak bond with alumina. β-alumina materials, which possess weak mica-like planes in their crystal structures, are phase-compatible with alumina, and their debonding characteristics are adequate. However, their use and fabrication temperatures are limited by morphological instability of the fiber/matrix interface (grain growth of the β-alumina platelets into the fibers).

1.0 Introduction

The goal of this research was to investigate and develop novel interphase materials for oxide–oxide composites that are stable in high temperature oxidizing environments, yet sufficiently weak to allow debonding as required for toughening. Such composites are needed to overcome the limitation of currently available nonoxide ceramic composites, which rely on layers of carbon or BN at the fiber–matrix interface for toughening, and thus are severely limited by oxidative degradation of the interfaces.

The initial work was directed at β-alumina materials, which we proposed as suitable interphases because of the weak mica-like planes in their crystal structures and their known compatibility with aluminum oxide (which is available as a reinforcing fiber and is a suitable matrix). The results are described in Section 3. Our experiments showed that, although as predicted, several β-alumina materials are phase-compatible with the sapphire fibers and their debonding characteristics are adequate, their use and fabrication temperatures are limited by morphological instability of the fiber/matrix interface (grain growth of the β-alumina platelets into the fibers). The problems of morphology seem to be difficult, maybe impossible to overcome. Two possible routes are (1) to keep processing temperatures and times sufficiently low that grain growth does not occur, (but that would probably limit the use temperature of the composites) and (2) to make all of the β-alumina platelets lie parallel to the surface of the fiber. Several methods we have tried showed some promise of achieving the latter: depositing crystalline magnetoplumbite (MP) on sapphire fibers from solutions of hexanoates of strontium or strontium and aluminum and vapor deposition of calcium and strontium on to the surface. In all cases, while much of the magnetoplumbite was flat on the surface, always about 10% was growing nearly normal to the surface which, as in the bulk, we take to be deleterious. Indeed, this is unfortunately the crystallographically preferred epitaxy with (110) of the β-alumina parallel to (001) of the fiber.

Studies of several other potential interface materials that are stable up to ~1300 to 1400°C and are compatible with alumina are also described in Section 3. $LaPO_4$ (monazite), CaF_2 (fluorite) and SnO_2 all exhibited weak bonding after being consolidated as a matrix with sapphire fibers. However, CaF_2 and SnO_2 (which was investigated previously by others) are not stable in aqueous and reducing environments, respectively. Results of a study of the reactions occurring in the

SnO_2–Al_2O_3 system in a reducing environment are described in Section 4. Neither TiO_2 nor $CaTiO_3$, both of which are compatible with Al_2O_3, exhibited useful debonding.

Sections 5 and 6 present detailed studies of interfacial fracture and high temperature stability of a variety of monazite–alumina composites. These studies demonstrate that monazite possesses all of the characteristics required of an interphase material for alumina–alumina composites, and most likely for many other combinations of ceramic matrix and fiber. It has a high melting point (2074°C); it is stable with alumina at high temperature in both oxidizing and slightly reducing environments (e.g., 1600°C in air for 20 hours); and it forms a sufficiently weak bond with alumina that cracks in the monazite cannot cross an interface into alumina because the interface debonds. In fiber sliding experiments in sapphire/monazite/alumina composites, debonding and sliding occurred cleanly at the interface between the monazite coating and the sapphire fiber. We hypothesize that this unusually weak bonding (which is essential for a composite interface) results from the particular crystal structure of monazite: the presence of the high-valent ion, P^{5+}, with a low coordination of four can satisfy a large portion of the valence bond to oxygen at a free surface, thus leading to weak bonding with other materials. To measure the stability and debonding characteristics, we fabricated a variety of composites, including monazite-coated sapphire fibers in alumina matrices, and multilayered monazite–alumina composites. Bulk monazite was also fabricated for measurement of thermophysical properties needed to analyze debonding characteristics. From its geological occurrence we expect monazite to be compatible with many materials including most silicates; we have preliminary results from several glasses, SiC, mullite, and ZrO_2. Therefore, the potential for monazite to overcome the major limitation of ceramic composites (namely the lack of oxidation resistance of the weak interface material) appears to be enormous.

2.0 Publications and Personnel

2.1 Publications

"Functional Interfaces for Oxide/Oxide Composites", P.E.D. Morgan and D.B. Marshall, *J. Mat. Sci. Eng.* **A162,** 15-25 (1993).

"Ceramic Composites of Monazite and Alumina for Stability in High Temperature Oxidizing Environments", P.E.D. Morgan and D.B. Marshall, submitted to *J. Amer. Ceram. Soc.*

"High Temperature Stability of Monazite–Alumina Composites", P.E.D. Morgan, D.B. Marshall and R.M. Housley, submitted to *J. Mat. Sci. Eng.*

"Some Effects of Eutectic Liquid under Reducing Conditions in the Alumina–Tin Dioxide Composite System", P.E.D. Morgan and R.M. Housley, in press, *Comm. J. Am. Ceram. Soc.*

"The Effect of Monazite Coatings on the Strength of Sapphire Fibers", P.E.D. Morgan, H. Childs and J.R. Porter, in preparation for *J. Amer. Ceram. Soc.*

"Monazite Coatings for Fiber Reinforced Composites by Laser Ablation", P.E.D. Morgan and J.T. Cheung, in preparation for *J. Amer. Ceram. Soc.*

2.2 Patent Applications

"Ceramic Composites having a Weak Interphase Material Selected From Monazites and Zenotimes", Morgan, P.E.D. and Marshall, D.B., U.S. patent application submitted.

2.3 Personnel

The principal investigators were Dr. P.E.D. Morgan and Dr. D.B. Marshall. Other contributors from Rockwell Science Center were Dr. J.R. Porter, Dr. R.M. Housley, Dr. J.T. Cheung and Mr. E.H. Wright. Two students, Mr. H. Childs and Ms. J. Dever, also worked on the project as part of the Science Center's Youth Motivation Program.

3.0 Functional Interfaces for Oxide/Oxide Composites

Published in the *Journal of Materials Science and Engineering*, **A162**, 15–25 (1993)

Materials Science and Engineering, A162 (1993) 15–25

Functional interfaces for oxide/oxide composites

Peter E. D. Morgan and David B. Marshall

Rockwell International Science Center, 1049 Camino Dos Rios, Thousand Oaks, CA 91360 (USA)

Abstract

Potentially useful interfacial coatings for composites of sapphire fibers in polycrystalline aluminum oxide matrices are discussed, subject to the constraints of phase compatibility in high temperature oxidizing environments and low mechanical interface strength (*i.e.* to allow pull-out). Results of preliminary tests to investigate feasibility of some candidate coatings (β-aluminas, $LaPO_4$ and CaF_2) are presented. These systems exhibited interfacial debonding under certain conditions, as required for high toughness composites, although several issues remain to be resolved before they can be used successfully.

1. Introduction

The more obvious requirements for a long-term, air-stable, high-temperature composite, consisting of a strong but brittle reinforcement in a brittle matrix are an interface or interphase between the fiber and matrix that is weak and stable over the entire range of use temperatures, chemical compatibility of the matrix/interphase/fiber system, environmental stability (especially mildly reducing to highly oxidizing), and low thermal expansion mismatch between fibers and matrix (but perhaps not always for the interphase material, as detailed later). Limitations in existing composites are the instability of presently known weak interfaces (*e.g.* carbon, boron nitride) in a high temperature oxidizing environment and the rare chemical (and/or morphological) compatibility of weak interphases with the fiber and matrix.

The interface must be sufficiently weak to allow debonding and sliding when a crack impinges upon it from the matrix; otherwise the crack passes through the fibers (or the fibers fail near the crack tip) and there is minimal or no toughening [1–6]. The relevant properties of the interface are defined by a debond energy Γ_i (of either the interphase material or the actual interfaces between the fibers, interphase material and matrix) and a shear stress τ that resists sliding of the debonded interface. He and Hutchinson [7] have shown that interfacial debonding occurs if Γ_i satisfies the condition $\Gamma_i/\Gamma_f \leqslant 0.25$, where Γ_f is the fracture energy of the fiber (this has long been known in fact [8]). Studies of ceramic composites with carbon and boron nitride interfaces, which satisfy this criterion, indicate that a notch-resistant response also requires that τ be less than about 100 MPa [9].

Here we concentrate on composites containing single-crystal alumina (corundum, sapphire) fibers (Saphikon®) in polycrystalline alumina matrices, as presently this is the only available oxidation-resistant monofilament fiber. However, certain generalities will apply to other conceivable future situations. For sapphire fibers, an interfacial debond energy $\Gamma_i \leqslant 5$ J m^{-2} is required [10]. Several potential interphase materials for this composite system have already been investigated. Refractory metals (Mo, Cr, W, Pt), which form relatively weak interfaces with alumina, and porous oxide coatings (ZrO_2, Al_2O_3), which have low fracture toughnesses because of their porosity, have been used to achieve debonding between sapphire fibers and Al_2O_3 matrices [10–12]. However, degradation of the fibers was observed with the Pt and some of the porous oxide coatings. Tin dioxide (SnO_2) has been used to provide a diffusion barrier and a weak interface between a glass matrix and both polycrystalline Al_2O_3 and sapphire fibers [13–15], and also in the case of the alumina single-crystal/alumina matrix [16a]. In the following sections other feasible interphase candidates will be discussed, and preliminary test results on these interphases in Al_2O_3/Al_2O_3 composites will be presented.

2. The choice of interphase materials

Amphoteric (exhibiting mixed basic and acid properties) alumina is phase compatible with few simple oxides because it can react readily with either acidic or basic oxides. This rules out simple oxides on the left- or right-hand sides of the conventional periodic table, leaving only a few compatible oxides of elements

0921-5093/93/$6.00

towards the center of the table, and especially lower down, such as SnO_2 [16b], ZrO_2 (and HfO_2), TiO_2 (below 1420 °C) and a few others which either are not sufficiently refractory (*e.g.* In_2O_3) or are easily reduced to metal. Another set of choices exists, however, in the mixed oxides, especially where an element from the left-hand side (basic) and an element from the right-hand side (acidic) form a fairly neutral mixed oxide, *e.g.* $BaSO_4$ (barite), $LaPO_4$ (molnazite), and perhaps a few others such as $CaTiO_3$ (perovskite). These are all well known in natural mineral assemblages with alumina. We previously found that $CaTiO_3$ is phase compatible with alumina [17]. Most other similar mixed oxides would not be sufficiently refractory, or would be either too strong in themselves or tending to bond too tightly with alumina.

Yet another possibility is that of a phase compatible refractory mixed aluminate oxide. However, most of these are also unsuitably strong for interphases. A conjectured exception is the refractory magnetoplumbite–β-alumina group [18]; these contain weak basal planes similar to those in brittle micas. The hexagonal β-alumina compounds consist of layers of spinel blocks $[Al_{11}O_{16}]^+$, with monovalent cations in interstices between the layers manifesting mainly ionic bonding. Several related structures (β, β'', β''', β^{iv}) differ by the number of oxygen layers in each spinel block (four or six), the specific ordering of cations between the blocks, and the stacking arrangement of the blocks.

While the existence of weak layers in the structure is somewhat analogous to that more familiar in for example a brittle mica, there are important differences: the number of elements in β-alumina is much smaller than is usual in a mica as, for example, in fluorophlogopite ($KMg_3(Si_3Al)O_{10}F_2$) which has previously been tried, but which has chemical compatibility problems [19]; this dramatically simplifies synthesis, phase relations and the quest for compatibility. The spinel layers are thicker than the aluminosilicate sheets in mica, thus usefully reducing the fraction of modifying cations. Most importantly for composites, many magnetoplumbite-β-alumina structures are stable in oxidizing atmospheres at temperatures up to about 1800 °C.

β-aluminas are members of an extended family of layer structures consisting of spinel block layers $[X_{11}O_{16}]^+$ (where $X \equiv Al^{3+}$, Ga^{3+}, Fe^{3+}, some Cr^{3+}, etc.) interleaved by a variety of weaker layers: those containing M^+ and O^{2-}, where M is typically Na^+, K^+ or other monovalent cations; $(MXO_3)^-$, where M is typically Ca^{2+}, Sr^{2+} etc. (but not Ba^{2+}, see below) or a 50:50 mix of monovalent and trivalent cations; $(MO_2)^-$ where M is La^{3+}, Nd^{3+}, etc. Therefore we have

$MO[X_{11}O_{16}]$ β-aluminas

$MXO_3[X_{11}O_{16}]$ normal magnetoplumbites

$MO_2[X_{11}O_{16}]$ rare earth related types

Other coupled substitutions between spinel blocks and interspinel layers are possible as for $M^{3+}XO_3[Z^{2+}X_{10}O_{17}]$, where $M^{3+} \equiv La^{3+}$, Nd^{3+}, etc. and $Z^{2+} \equiv Mg^{2+}$, Co^{2+}, Ni^{2+}, etc. Previous work details some of the extensive solid state chemistry of this group [20].

Of immediate concern here is the β-alumina case. The mechanically weak, open layer alkali-containing layers are spaced about 11.5 Å apart. These layers support fast ionic transport of the monovalent ions, which, among other contemplated uses, has been greatly desired for Na/S batteries. Unfortunately, after 35 years of research, the very same layers, which are very weak, remain a feature limiting the strength of β-alumina ceramics, most especially at large grain size, so that economical and practical batteries have not been achieved to date, although research continues. Na–β-alumina weak layers have also been found to degrade the lifetime of Lucalox® when it forms in that alumina used in high pressure Na lamps. The β types $NaAl_{11}O_{17}$ or $KAl_{11}O_{17}$, or closely related β'' types such as $Na_2MgAl_{10}O_{17}$ or $K_2MgAl_{10}O_{17}$, which differ mainly in the spinel block stacking order, are all phase compatible with Al_2O_3 (or rather with alumina containing Na or K in saturated solid solution).

The sodium-containing compounds are not the most desirable candidates here because the solubility of Na in Al_2O_3 must be fairly high; typical commercial aluminas contain approximately 0.02% Na, yet crystalline $NaAl_{11}O_{17}$ is not generally reported as being present in these fired powders or ceramics. This is not surprising as the ionic radius of Na^+ (in VI coordination) is 1.16 Å and Mg^{2+}, at 0.86 Å, is known to be appreciably soluble in Al_2O_3.

More interesting are the potassium analogs. By virtue of its much larger ionic radius (1.52 Å), the solubility of K^+ is immeasurably small; a key observation of the precipitation of platelets of K–β-aluminas in alumina containing very low levels of K has been reported [20]. The stability and detectability of these phases are also increased by the presence of low levels of Mg^{2+} (often added as a sintering aid) which stimulates the formation of β''' (approximately $KMg_2Al_{15}O_{25}$) and yet other related species. In the K case then we have a compound that forms easily and persists at high temperatures, with mechanically weak layers, that is compatible with alumina [21] and should therefore be an ideal weak interfacial material between alumina fibers and several matrices including alumina and $MgAl_2O_4$ spinel.

Ba^{2+} might be expected to form the normal $MXO_3[X_{11}O_{16}]$ magnetoplumbite type but, because the Ba ionic radius is so large, this idealized magnetoplumbite

structure is not found; instead, its compounds, which may also contain Mg, tend towards the more open weaker layer β-types [22] and are therefore also candidates.

Thus, the ease of formation, compatibility, and weak layers of the β-aluminas, which have heretofore bedeviled the fabrication of satisfactory ceramics of these materials, suggested making "virtue out of necessity" by using them as the weak interfaces between alumina fibers and host aluminous matrices.

Aside from compounds already containing oxygen, only a few fluorides are sufficiently oxidation resistant, phase compatible with alumina (*e.g.* CaF_2 and perhaps LaF_3), refractory and soft enough to be possible candidates as interphase materials.

3. Experimental details

3.1. Synthesis and fabrication of test specimens

All the magnetoplumbite(MP)-β-alumina group compounds were made by a tried and tested "chemical" method [20]. To a thick blending slurry of Dispersal®, AlO(OH), the appropriate quantities of mixed aqueous solutions of nitrates or acetates of the other cations were quickly added; this caused the slurry to thicken even further. The mixtures were dried in a vacuum oven at about 120 °C and then fired to various temperatures between 1200 °C and 1600 °C overnight to form the MP-β-compounds which were then ground in an alumina ball mill and sieved to less than 200 mesh. K-β'''-alumina, $KMg_2Al_{15}O_{25}$, $CaAl_{12}O_{19}$, "$CaMgAl_{14}O_{23}$", "$BaMg_2Al_{16}O_{27}$", "$Ba_{0.5}Mg_{0.5}Al_{16}O_{27}$", $(BaO)_{1.1}Al_{10.5}Mg_{1.1}O_{17.15}$ (a Philips lamp phosphor composition), $Ba_{0.82}Al_{12}O_{18.82}$ (known as type-1) [22], $Ba_{1.3}Al_{12}O_{19.3}$ (known as type-2) [22], "$Ba_{0.3}Mg_{0.3}Al_{14}O_{21.6}$", "$BaMgAl_{14}O_{23}$" and others were all made up in this way. Samples in quotes were attempts to make new types and included unusual firing schedules [23a]. Several samples were also made by standard ball-milling–mixing from carbonates, solid acetates and AlO(OH). Other powders were obtained commercially.

For preliminary assessment, consolidation of the test specimens was done by placing Saphikon fibers in a matrix of the specific powder and hot-pressing at temperatures of 1200–1600 °C in graphite die sets under nitrogen. The fibers were approximately 60 μm in diameter with a rounded triangular cross-section. Other specimens were fabricated with sapphire plates, and others with polycrystalline Al_2O_3 matrices and coatings applied to the fibers by dipping in a slurry of the powder.

3.2. Fracture testing

Several test specimens, Fig. 1, were used for qualitative and quantitative evaluation of interfacial debonding. For simple screening of interfaces to determine whether or not interfacial debonding occurred, a surface was polished normal to the interface and a Vickers indenter was loaded onto the surface near the interface as shown in Fig. 1(a). The radial indentation cracks, which grew toward the interface, either deflected into the interface if it was sufficiently weak, or penetrated into the fiber if the interface was strong. In specimens that exhibited interfacial debonding, the tests illustrated in Fig. 1(b)-(d) were used for further evaluation of the interfacial properties. The effect of mode I crack growth normal to fibers was assessed as in Fig. 1(b). The interfacial sliding resistance τ in specimens that contained fibers was evaluated using the indentation test of Fig. 1(c) [23b].

$$\tau = F^2/4\pi^2 u R^3 E_f \quad (1)$$

where $u = (b-a)\cot\psi$, b and a are the indentation dimensions indicated in Fig. 1(c), F is the force applied to the fiber, ψ is the angle between opposite edges of the indenter ($\psi = 70°$ for the Vickers indenter), R is the fiber radius, and E_f is the Young modulus of the fibers. Finally, debonding along planar interfaces under mixed mode loading was evaluated using the test specimen of Fig. 1(d) [24].

4. Results and discussion

4.1. β-alumina related materials

4.1.1. Single-crystal experiments: Na(Li)-β″-alumina

The anisotropy in fracture toughness of Na(Li)-β''-alumina was investigated using indentation fracture. Small single crystals [25] (approximately $1 \times 1 \times 0.1$ mm^3) were polished normal to the basal plane, and indented with a Vickers pyramid aligned with its diagonals parallel and normal to the basal plane. This caused extensive cracking on the basal planes, but only occasional small cracks in the perpendicular direction (Fig. 2(a)), indicating a much smaller fracture toughness on the basal plane, as anticipated from consideration of the crystallography (Section 2). The small fracture toughness of the basal planes was also evident from the ease of cleavage: the crystals were readily cleaved into very thin sheets by pressing with a sharp needle and were very similar in response to mica.

The sizes of the cracks parallel and normal to the basal plane in Fig. 2(a) can be used to estimate the corresponding relative fracture toughnesses, using the indentation fracture mechanics relation [26, 27]

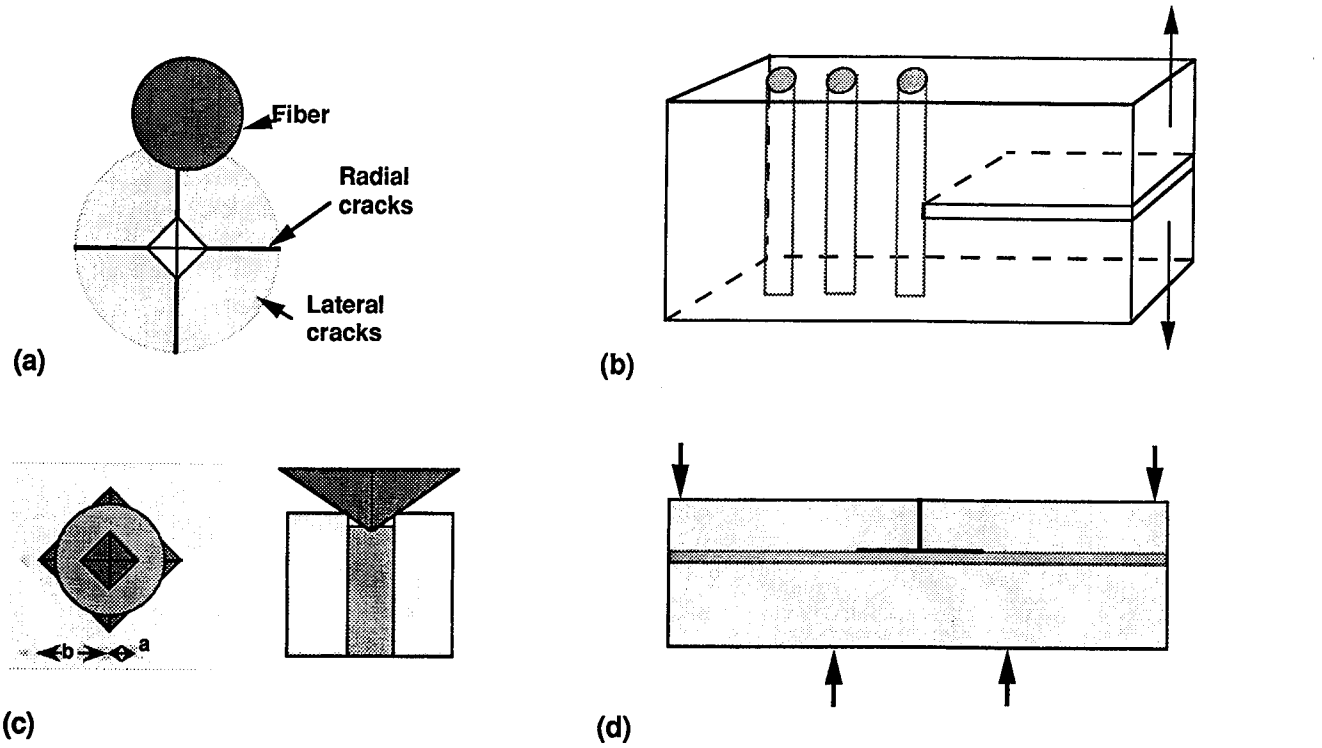

Fig. 1. (a) Cracks generated by Vickers indentation. (b) Growth of macroscopic mode I crack on plane normal to fibers. (c) Interface sliding caused by indentation on end of fibers (ref. 23b). (d) Interfacial debonding under flexional loading (ref. 24).

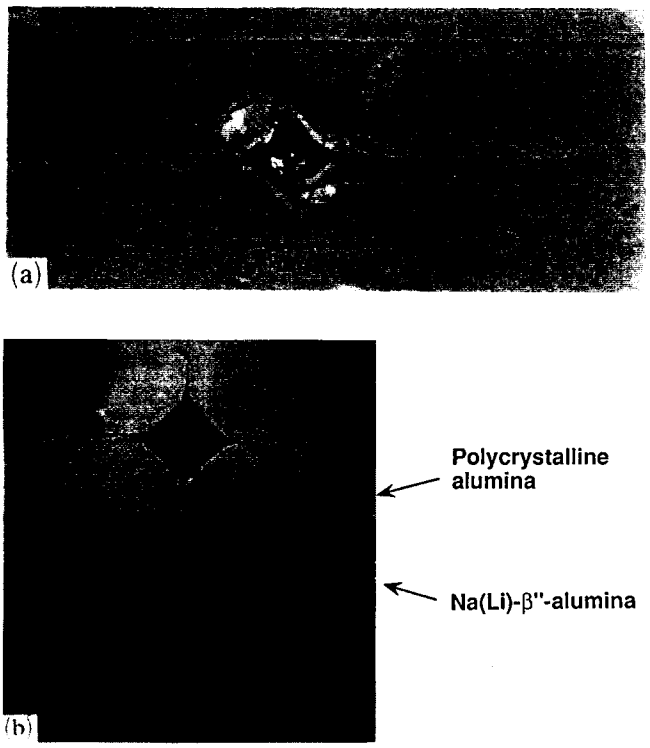

Fig. 2. (a) Vickers indentations in single-crystal Na(Li)-β''-alumina, cracks are parallel to the basal plane; (b) Vickers indentation in polycrystalline Al_2O_3 matrix adjacent to single-crystal Na(Li)-β''-alumina inclusion.

$K \propto c^{-3/2}$, where K is the fracture toughness and c is the crack length. Data from ten indentations in several crystals gave $K_b/K_n = 0.1$, where the subscripts b and n denote planes parallel and normal to the basal plane. Similar results have been obtained previously by Hitchcock and DeJonghe [28] in Na-β-alumina. This ratio of fracture toughnesses (which correspond to a ratio of fracture energies of 0.01) easily satisfies the debonding criterion of the analysis of He and Hutchinson [7], and therefore suggests that a crack lying on a plane parallel to the c-axis should deflect into the basal plane rather than continue to grow normal to it.

To test the effectiveness of this material as a weak interphase, some of the crystals were embedded in a polycrystalline alumina matrix (by hot pressing Al_2O_3 powder around the Na(Li)-β''-alumina crystals). The composite was sectioned and polished on a plane normal to the basal plane of the crystals, and the polished surface was indented with a Vickers pyramid in the polycrystalline matrix near the Na(Li)-β''-alumina crystal (Fig. 2(b)). The radial crack that was incident upon the crystal in a direction normal to the basal plane arrested by splitting parallel to the basal plane after growing into the crystal to a depth of approximately 10 μm.

Whereas the results in Fig. 2 confirm the potential for β-alumina crystals to provide weak interfacial

layers in composites, they also pose a question. If the fracture toughness of the basal plane is sufficiently small to satisfy the criterion for debonding, then crack growth normal to the basal plane should be limited to the thickness of a single spinel block of the β-alumina structure, rather than being 5–10 μm as observed in Fig. 2. The observed response suggests some non-uniformity in the crystal structure (*e.g.* polytypes). Transmission electron microscopy is being used to determine whether the structures of the planes that exhibit splitting in Fig. 2 differ from that of the remainder of the crystal.

4.1.2. $BaMg_2Al_{16}O_{27}$

As an initial assessment of the anisotropy in fracture properties of $BaMg_2Al_{16}O_{27}$ crystals, a polycrystallline specimen which, unexpectedly, contained some unusually large lath-shaped grains (Fig. 3(a) and (b)) was fabricated by hot pressing at 1700 °C under the usual nitrogen conditions. Suspecting that this unusual effect was related to water loss (the specimen had AlO(OH) in the starting mixture) and subsequently using a vacuum method revealed that the anisotropic large laths were exaggerated still further. A notched beam test specimen of this sample was fractured by loading in four-point bending. The fracture toughness thus measured was approximately 2 MPa $m^{1/2}$, smaller than that of polycrystalline alumina (about 4–6 MPa $m^{1/2}$). The fracture surface comprised mostly cleavage fracture along the basal planes of the large lath-shaped grains, thus accounting for this relatively low value. Moreover, many of the facets were oriented at high angles (up to 90°) relative to the direction of growth of the main crack, indicating that the basal planes of the large lath-shaped grains are indeed sufficiently weak to cause deflection of a normally incident crack (Fig. 3(c)).

The ability of $BaMg_2Al_{16}O_{27}$ to protect sapphire fibers from cracking was assessed by fabricating composites containing isolated sapphire fibers in this matrix, and observing the interfacial microstructure and response to indentation cracking. In composites fabricated in the normal way by hot pressing at 1700 °C, the matrix was similar to that of Fig. 3(a), with large laths (approximately 200 μm length by 1 μm thickness) of $BaMg_2Al_{16}O_{27}$. The laths tended to form envelopes around the fibers, with the basal planes aligned with the fiber surfaces (Fig. 4), as might be desired for optimum deflection of cracks. However, there was also growth of laths into the fibers and growth of the fibers into the matrix, both of which must degrade the strength of the fibers. The observations indicate that although the $BaMg_2Al_{16}O_{27}$ is chemically phase compatible with the sapphire fibers, the two systems are not morphologically stable at temperatures where extensive grain growth occurs. The effectiveness

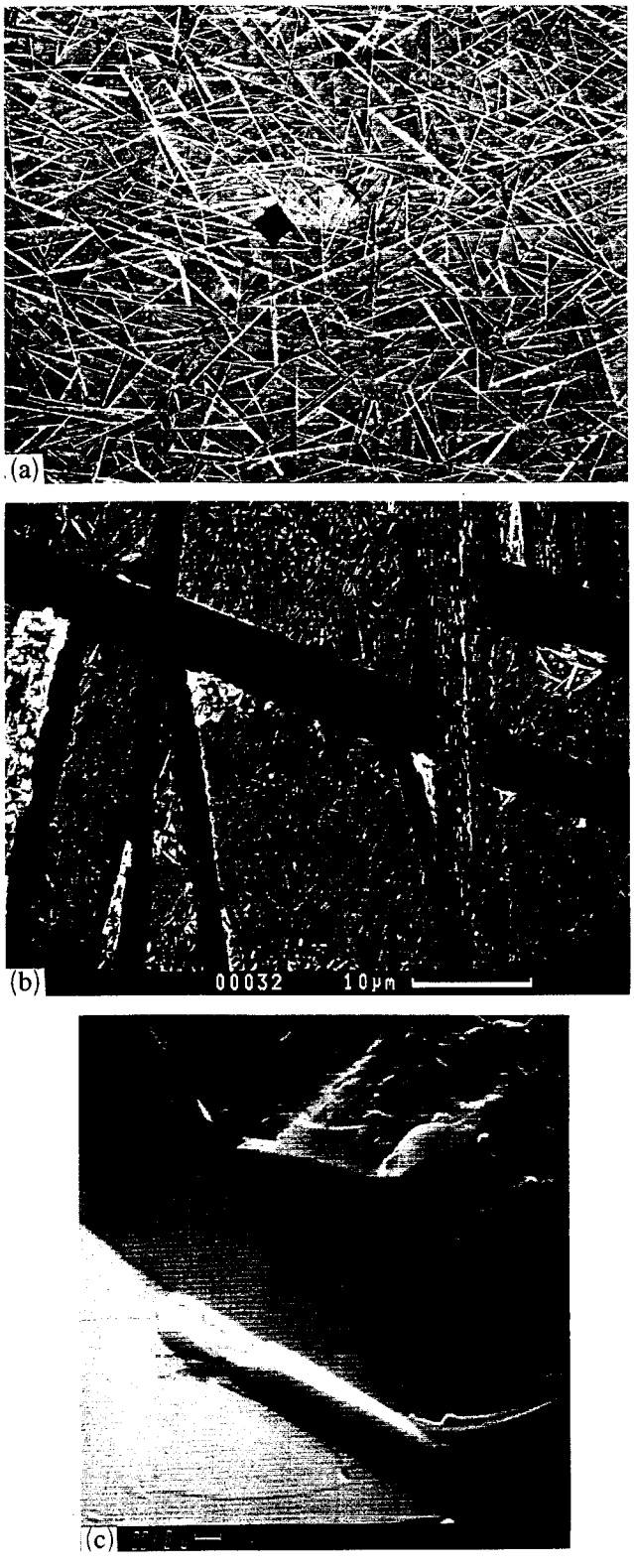

Fig. 3. (a) Optical micrograph of polycrystalline $BaMg_2Al_{16}O_{27}$ showing large platelets developed by hot pressing specimen in higher vacuum at 1700 °C. (b) Higher magnification of (a), showing fine grained microstructure between the long laths. (c) Scanning electron micrograph of fracture surface from notched beam specimen of material shown in (a) (direction of crack growth is from bottom left to top right).

Fig. 4. Optical micrograph showing sapphire fiber in matrix of $BaMg_2Al_{16}O_{27}$, fabricated by hot pressing at 1700 °C under low nitrogen pressure.

of the envelopes of laths surrounding the fibers at deflecting indentation cracks was mixed. In some cases, such as shown in Fig. 4, the cracks were deflected, whereas in others the cracks penetrated into the fibers, especially when the crack ran along a lath that was oriented with its basal plane normal to the fiber surface.

In an attempt to avoid the morphological instability, composites were fabricated at lower hot pressing temperatures: 1650 °C, 1450 °C and 1300 °C. At 1650 °C and 1450 °C the grain size of the matrix was smaller and the surface of the fiber did not appear to be damaged (at the resolution of the scanning electron microscope). However, indentation cracks in the matrix penetrated into the fibers. In the composite fabricated at 1300 °C the indentation cracks did not penetrate the fibers. However, the $BaMg_2Al_{16}O_{27}$ matrix was not fully dense (about 20% porosity). Therefore, we cannot tell whether it was the low density or the intrinsic weakness of the basal planes that was responsible for the crack deflection in this case. Further study of this system using techniques for obtaining a fully dense matrix at temperatures below 1300 °C appears to be warranted.

4.1.3. $KMg_2Al_{15}O_{25}$-β'''-alumina

To evaluate the effectiveness of $KMg_2Al_{15}O_{25}$ in protecting sapphire fibers from fracture, composites containing isolated fibers in a matrix of polycrystalline $KMg_2Al_{15}O_{25}$ were fabricated by hot pressing at several temperatures (1625 °C, 1450 °C and 1300 °C). The composites fabricated at 1625 °C were further annealed at the same temperature for 15 h to promote coarsening of the microstructure. This caused growth of platelets approximately 1 μm thick and 10 μm in diameter (Fig. 5), a smaller aspect ratio than in the $BaMg_2Al_{16}O_{27}$. It also caused growth of the platelets into the fibers and/or growth of the fibers into the matrix, thus degrading the fibers. The platelets were effective in some cases in preventing growth of indentation cracks into the fibers, but generally the cracks penetrated the fibers as shown in Fig. 5.

The composites that were hot pressed at lower temperatures were porous and the grain sizes were smaller. Indentation cracks penetrated into the fibers in the composite that was hot pressed at 1450 °C, but not in the composite that was pressed at 1300 °C. However, as in the case of $BaMg_2Al_{16}O_{27}$, we do not know whether this is due to the low density of the matrix or the intrinsic weakness of the β-alumina crystal structure. This specimen was also tested by growing a macroscopic crack normal to the fibers, as in Fig. 1(b). A small amount of fiber pull-out occurred. However, the pull-out lengths were less than a fiber diameter, indicating that either the fiber strength was severely degraded or debonding was rather limited.

Another composite with a matrix that was slightly richer in Al_2O_3, attempting to ensure chemical compatibility, was fabricated in an attempt to prevent growth of the laths of matrix into the fibers. This matrix was effective in preventing growth of matrix cracks into the fibers in most cases, but not always.

4.2. $LaPO_4$ (monazite)

Monazite is found in association with corundum in natural rocks. Tests on powders as high as 1550 °C confirmed this phase compatibility with no melting. A composite consisting of a polycrystalline $LaPO_4$ matrix with isolated sapphire fibers was fabricated by hot pressing at up to 1355 °C. The desirable softness of the $LaPO_4$ matrix, however, caused difficulty in polishing a very smooth surface in the matrix adjacent to the fibers and in generating clearly visible indentation cracks in the matrix. Therefore, instead of indenting the matrix adjacent to the fibers to generate cracks, the fibers were indented with the Vickers pyramid. This caused cracks within the fiber, which appeared to arrest at the interface. It also caused sliding of the fibers, indicating that the fiber–matrix interface is sufficiently weak to allow debonding. An indentation load of 20 N on a

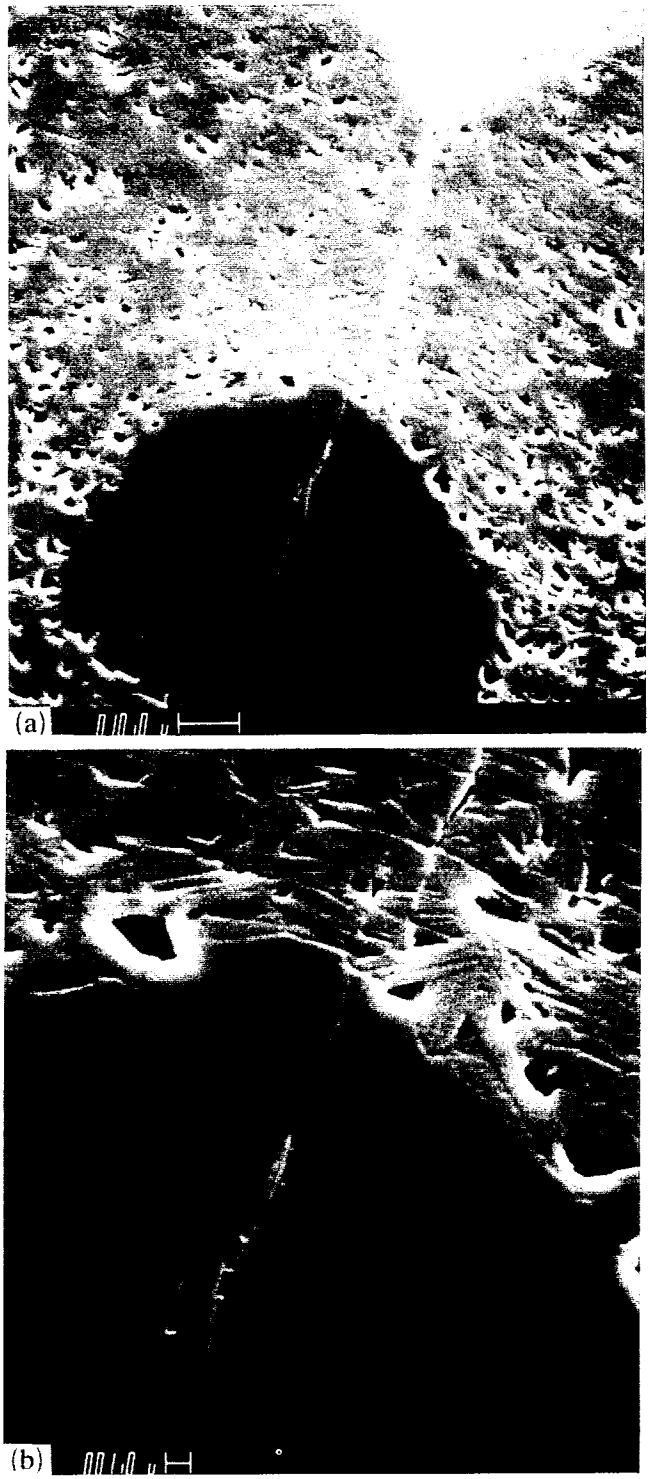

Fig. 5. (a) and (b) scanning electron micrographs showing effect of morphological instability of interface between the sapphire fiber and $KMgAl_{15}O_{25}$ (β'''-alumina) matrix. The crack from the Vickers indentation at the top of (a) penetrates the fiber.

60 μm diameter fiber caused 10 μm displacement of the top of the fiber below the surface of the matrix. Using eqn. (1), this implies an upper bound of 60 MPa for the interfacial sliding resistance. Preliminary X-ray data indicate some solid solution of Al_2O_3 in $LaPO_4$ so this needs further attention.

4.3. CaF_2 (fluorite)

Three types of specimen were fabricated to evaluate CaF_2 (believed to be phase compatible with alumina [29] and certainly found together with it in nature) as an interphase material. Sapphire fibers were embedded within a matrix of polycrystalline CaF_2 by hot pressing at 1250 °C. A eutectic exists at 1395 °C [29]. Sapphire fibers were also coated with CaF_2 by dipping in a slurry of the powder, and embedded in a matrix of polycrystalline Al_2O_3 by hot pressing at 1300 °C. The third specimen was a sandwich of single-crystal-sapphire-plate/CaF_2/single-crystal-sapphire-plate, fabricated by placing CaF_2 powder between the plates, surrounding them with Al_2O_3 powder, and hot pressing at 1300 °C.

The CaF_2 layer in the planar sandwich specimen was approximately 100 μm thick and contained a small amount of porosity at grain boundaries. The grains had grown through the entire layer and their size in the plane of the layer was about 100 μm. The layer was cracked after fabrication because of the large mismatch in thermal contraction; the thermal expansion coefficients over the relevant temperature range are approximately $(20\text{–}30)\times10^{-6}$ K^{-1} for CaF_2 and approximately 8×10^{-6} K^{-1} for Al_2O_3. Growth of a crack from the sapphire to the interface caused debonding of the specimen as indicated in Fig. 6, with reasonably clean separation between the CaF_2 and the sapphire, although remnants of CaF_2 adhered to the sapphire surface in some places (Fig. 6(c)). Such debonding, due to the mismatch in coefficient of thermal expansion, could be of some utility in producing weak interfaces. X-ray diffraction from the debonded sapphire surface and from sapphire disks treated for various times in powders of CaF_2 showed various products at low levels including $CaAl_{12}O_{19}$ (hibonite), $CaAl_4O_7$ and even unknown structures. The suspicion is that CaF_2 and Al_2O_3 are truly phase compatible in a closed system, but that in oxygen and even more likely in water vapor, some loss of fluorine can occur leading to these compounds.

In the composite containing sapphire fibers in a matrix of CaF_2, damage caused by polishing in the surface of the matrix near the interface prevented direct observation of the interaction of indentation cracks with the interface and also interfered with measurements of the indentation dimension b in Fig. 1(b) in fiber pushing tests. However, sliding of the fibers during pushing experiments was detected using optical interference microscopy to measure the residual displacement of the fiber surface below the matrix after unloading the indenter. Assuming that the residual displacement is half of the peak-load displacement

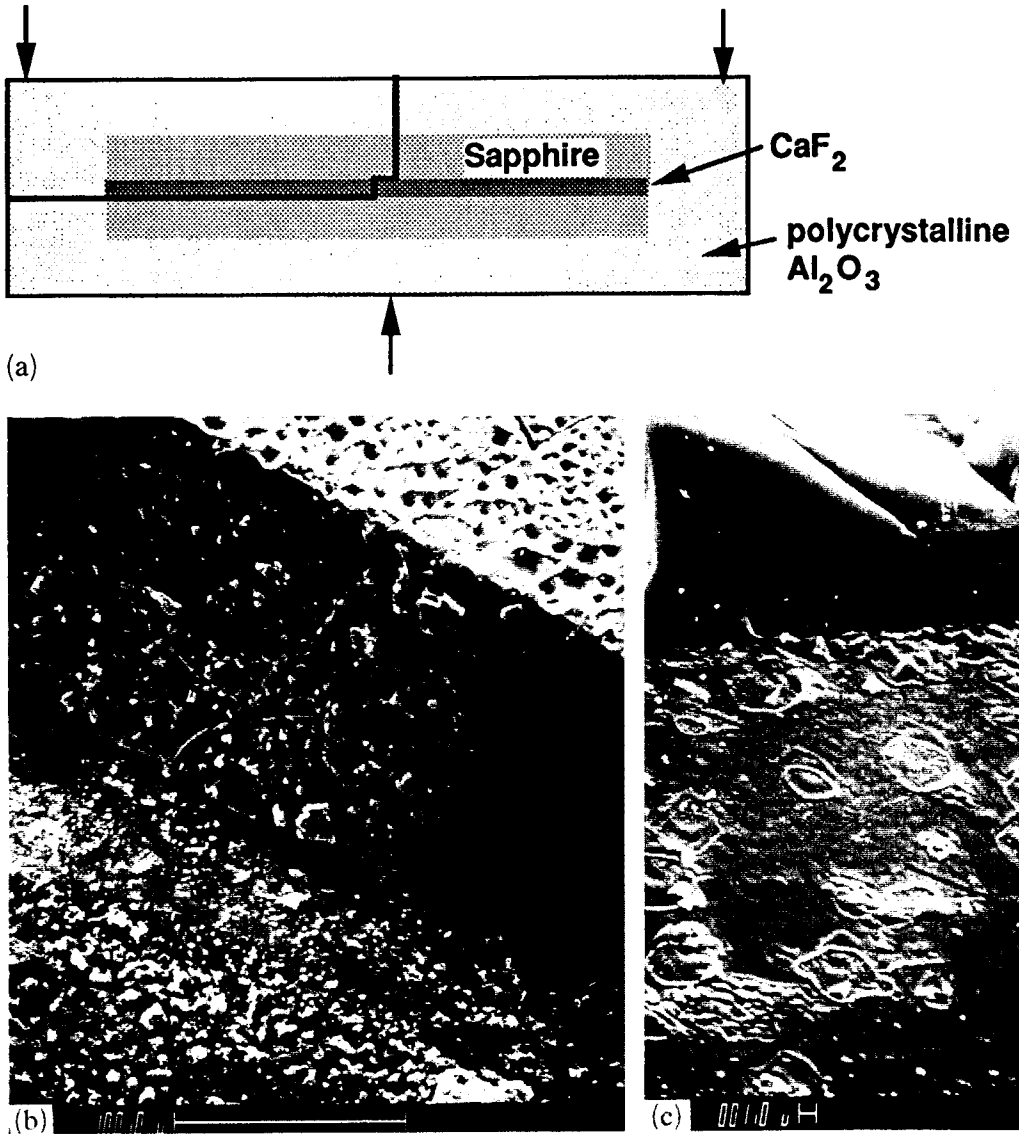

Fig. 6. (a) Schematic diagram of planar specimen containing a layer of CaF_2 sandwiched between plates of sapphire, all embedded within a polycrystalline Al_2O_3 matrix. (b) (c) Scanning electron micrographs showing fracture surface after debonding as indicated in (a).

(a result that holds strictly only for fibers that are free of residual stresses), the frictional sliding resistance calculated from eqn. (1) is 20 ± 10 MPa. This is within the range expected to be suitable for effective reinforcement of composites. The growth of mode I cracks normal to the fibers as in Fig. 1(b) caused a large amount of fiber debonding and pullout (Fig. 7).

The CaF_2 coating in the composite with a polycrystalline Al_2O_3 matrix was not very uniform: the thickness varied between zero and about 5 μm, with most of the fiber surface being covered. However, there were small areas that apparently had no coating. The coating was effective in arresting and deflecting indentation cracks that were incident on the interface either from the matrix or from within the fiber (Fig. 8). However, fiber sliding due to indentation on the end of the fiber was not detected, presumably because of strong bonding in regions beneath the surface, where the surface coating might be missing. For the same reason, fiber pull-out was not observed on a fracture surface normal to the fibers (as in Fig. 1(b)). Improvements in the uniformity of the fiber coating would be expected to improve these results.

4.4. LaF_3 (fluocerite-(La))

LaF_3 appears to be phase compatible with Al_2O_3, although no phase diagram was found. High temperature tests with mixed powders of Al_2O_3 and LaF_3

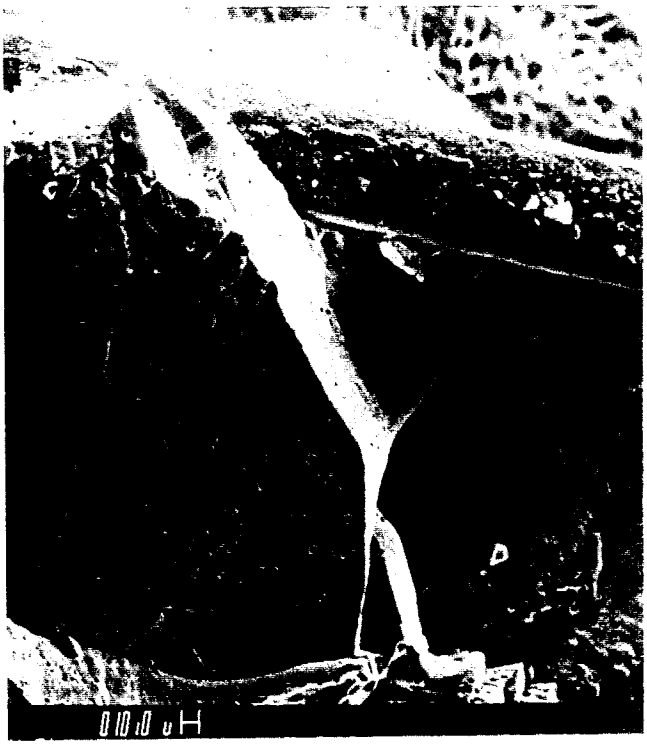

Fig. 7. Scanning electron micrograph showing debonding and pull-out of sapphire fiber in matrix of CaF_2 after growing a mode I crack through the matrix.

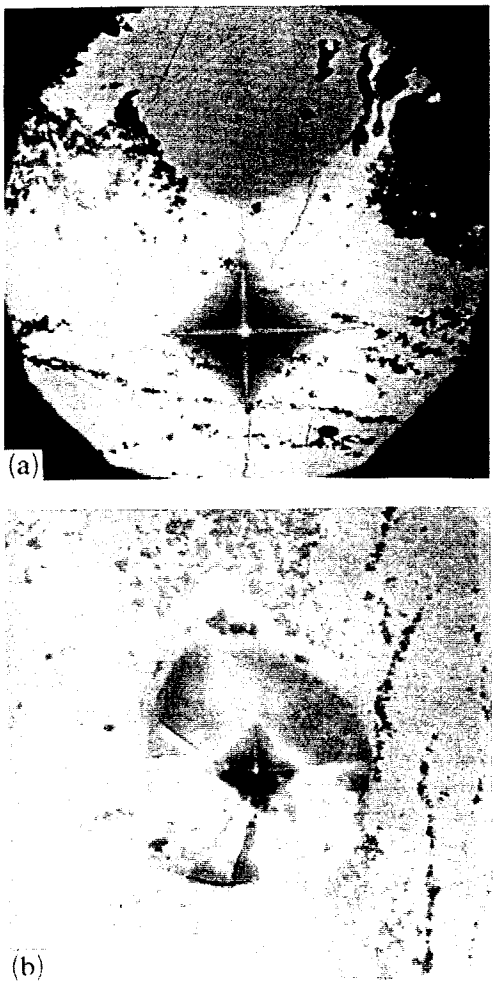

Fig. 8. Optical micrographs of coated (CaF_2) sapphire fibers in polycrystalline Al_2O_3 matrix showing crack arrest and/or debonding at the interface: (a) indentation in matrix, (b) indentation in fiber.

suggested that LaF_3 might prove to be more appropriate than CaF_2 because LaF_3 appears only to convert a little to LaOF which also appears to be phase compatible with Al_2O_3. No compounds such as $LaAl_{11}O_{18}$ were noted. In preliminary work this also appears to be a promising candidate.

4.5. SnO_2 (cassiterite)

Briefly, to test whether SnO_2, which is known to be phase compatible with Al_2O_3 [16b], soft and refractory, eutectic at 1620 °C, and already tested in alumina/alumina composites [16a], is a suitable interface, we hot pressed sapphire fibers into an SnO_2 matrix in oxygen. Figure 9 shows that, indeed, debonding, occurred. Moreover, sapphire plates sintered in air with SnO_2 sandwiched in between simply fell apart; X-ray diffraction on these indicated no reaction at all. The problem here is that composites in this system could never be exposed even to a slightly reducing environment as the melting point of the lower oxide, SnO, is only 1080 °C and eutectics are presumably lower. In a situation where only oxidizing atmospheres are to be encountered, such as in the glass industry, then there may be a use for an Al_2O_3 fiber/SnO_2 matrix composite.

4.6. TiO_2 (rutile), $CaTiO_3$ (perovskite) and $BaSO_4$ (barite)

As mentioned earlier, TiO_2 does not react with Al_2O_3 below 1420 °C; sapphire fibers hot-pressed into a titania matrix confirmed this with no visible attack, but tests indicated that the matrix and interface are too strong to produce the desired crack conformations. A similar preliminary situation was found with $CaTiO_3$. $BaSO_4$, where no phase diagram with alumina could be found, does in fact react as seen in powder mixture tests and so is out of the picture.

5. Conclusions

The constraints of mechanical weakness, high temperature chemical compatibility and stability in oxi-

Fig. 9. Groove remaining in SnO_2 matrix after fracture caused debonding and removal of a sapphire fiber.

dizing environments limit the choices of interfacial coatings for Al_2O_3/sapphire composites. Several possibilities in addition to the refractory metal, porous oxide and SnO_2 coatings already in the literature are proposed. These include $LaPO_4$, CaF_2, and perhaps LaF_3, and crystal structures from the magnetoplumbite-β-alumina group which possess weak mica-like basal planes.

β-alumina materials allowed debonding. However, although they are chemically compatible with Al_2O_3, fiber degradation was caused by morphological instability of the interface, due to grain growth during fabrication and high temperature annealing. Low temperature processing routes or additional diffusion barrier coatings will be needed to prevent fiber degradation.

Debonding of CaF_2–Al_2O_3 interfaces was observed, although there is some concern about decomposition of CaF_2 in high-temperature, water-containing environments. Debonding and cracking of CaF_2 coatings were enhanced by residual stresses caused by the large mismatch in thermal expansion coefficients of CaF_2 and Al_2O_3. A similar mismatch exists for LaF_3 which appears to be more compatible with Al_2O_3. Debonding was also observed in $LaPO_4$ and SnO_2 matrices which contained sapphire fibers. However, neither TiO_2 nor $CaTiO_3$ matrices have yet exhibited useful debonding although the results are preliminary.

Acknowledgments

Funding for this research was provided by the US Office of Naval Research, Contract No. N00014-91-C-0157, and by the Rockwell International Independent Research and Development Fund and the Youth Motivation Fund. The authors are grateful to E. H. Wright and J. D. Piché for assistance with specimen preparation, to R. R. Neurgaonkar and J. G. Nelson for the hot-pressing of SnO_2 in oxygen, and to J. R. Porter for supplying the micrographs in Fig. 3(b) and (c).

References

1 T. A. Michalske and T. R. Hellmann, Strength and toughness of continuous-alumina-fiber-reinforced glass-matrix composites, *J. Am. Ceram. Soc., 71* (1988) 725–731.
2 J. Aveston, G. A. Cooper and A. Kelly, *Properties of Fibre Composites*, IPC Science and Technology, London, 1971.
3 D. B. Marshall and A. G. Evans, Overview no. 85, The mechanical behavior of ceramic matrix composites, *Acta Metall. Mater., 37* (1989) 2567–2583.
4 L. R. F. Rose, Effective spring constant for unbroken ligaments between crack faces, *Int. J. Fracture, 33* (1987) 145–152.
5 D. B. Marshall, B. N. Cox and A. G. Evans, The mechanics of matrix cracking in brittle-matrix fiber composites, *Acta Metall. Mater., 33* (1985) 2013–2021.
6 B. Budiansky, J. W. Hutchinson and A. G. Evans, Matrix fracture in fiber-reinforced ceramics, *J. Mech. Phys. Solids, 34* (1986) 167–184.
7 M.-Y. He and J. W. Hutchinson, Crack deflection at an interface between dissimilar materials, *Int. J. Solids Struct., 25* (1989) 1053–1067.
8 J. E. Gordon, *The New Science of Strong Materials*, Penguin, London, 1968, p. 114.
9 H. C. Cao, E. Bischoff, O. Sbaizero, M. Rühle, A. G. Evans, D. B. Marshall and J. J. Brennan, Effect of interfaces on the properties of fiber-reinforced ceramics, *J. Am. Ceram. Soc., 73* (1990) 1691.
10 J. B. Davis, J. P. A. Lofvander, A. G. Evans, E. Bischoff and M. L. Emiliani, Fiber coating concepts for brittle matrix composites, *J. Am. Ceram. Soc.*, in press.
11 M. H. Jaskowiak, J. I. Eldridge, J. B. Hurst and J. A. Setlock, Interfacial coatings for sapphire/Al_2O_3. In *High Temp. Rev. 1991*, NASA Conference Publication 10082, 1991, p. 84.
12 J. B. Davis, E. Bischoff and A. G. Evans, Zirconia coatings for sapphire fiber-reinforced composites. In M. D. Sacks (ed.), *Advanced Composite Materials*, American Ceramic Society, 1991, pp. 631–638.
13 A. Maheshwari, K. K. Chawla and T. A. Michalske, Behavior of interface in alumina/glass composite, *Mater. Sci. Eng., A107* (1989) 269.
14 M. Siadati, K. K. Chawla and M. K. Ferber, The role of the SnO_2 interphase in an alumina/glass composite: a fractographic study, *J. Mater. Sci., 26* (1991) 2743.
15 R. Venkatesh and K. K. Chawla, Effect of interfacial roughness on fiber pullout in alumina/SnO_2/glass composites, *J. Mater. Sci. Lett., 11* (1992) 650–652.
16 (a) M. E. Norkitis and J. R. Hellmann, Evaluation of SnO_2 interfacial coatings for sapphire reinforced alumina com-

posites. In *High Temp. Rev. 1991*, NASA Conference Publication 10082, 1991, p. 85.
(b) V. J. Barczac and R. H. Insley, Phase equilibria in the system Al_2O_3–SnO_2, *J. Am. Ceram. Soc., 45* (1962) 144.
17 P. E. D. Morgan and M. S. Koutsoutis, Phase relations in the Ca–Ti–Al–O system: further studies on members of the CTA family, *J. Mater. Sci. Lett., 4* (1985) 321–323; erratum 5 (1986) 122–124.
18 R. Collongues, D. Gourier, A. Kahn-Hanari, A. M. Lejus, J. Théry and D. Vivien, Magnetoplumbite related oxides, *Ann. Rev. Mater. Sci., 20* (1990) 51–82.
19 R. F. Cooper and P. C. Hall, Reactions between synthetic mica and simple oxide compounds with application to oxidation-resistant ceramic composites, *J. Am. Ceram. Soc.*, in press.
20 P. E. D. Morgan and J. A. Miles, Magnetoplumbite-type compounds: further discussion, *Commun. Am. Ceram. Soc., 69* (1986) C157–C159.
21 M. Blanc, A. Mocellin and J. L. Studd, Observation of potassium β-alumina in sintered alumina, *J. Am. Ceram. Soc., 60* (1977) 403–409.
22 P. E. D. Morgan and T. M. Shaw, Magnetoplumbite related barium aluminates, *Mater. Res. Bull., 18* (1983) 539–542.
23 (a) P. E. D. Morgan, Preparing new extremely-difficult-to-form crystal structures, *Mater. Res. Bull., 19* (1984) 369–376.
(b) D. B. Marshall, An indentation method for measuring matrix–fiber frictional stresses in ceramic composites, *J. Am. Ceram. Soc., 67* (12) (1984) C259–C260.
24 P. G. Charalambides, H. C. Cao, J. Lund and A. G. Evans, Development of a test method for measuring the mixed mode fracture resistance of bimaterial interfaces, *Mech. Mater., 8* (1990) 269–283.
25 B. Dunn, B. B. Schwartz, J. O. Thomas and P. E. D. Morgan, Preparation and structure of Li-stabilized Na^+–β''-alumina single crystals, *Solid State Ionics, 28–30* (1988) 301–305.
26 B. R. Lawn, A. G. Evans and D. B. Marshall, Elastic plastic indentation damage in ceramics, the median/radial crack system, *J. Am. Ceram. Soc., 63* (9–10) (1980) 574–581.
27 G. R. Anstis, P. Chantikul, B. R. Lawn and D. B. Marshall, A critical evaluation of indentation techniques for measuring fracture toughness: I, direct crack measurements, *J. Am. Ceram. Soc., 64* (9) (1981) 533–538.
28 D. C. Hitchcock and L. C. DeJonghe, Fracture toughness anisotropy of sodium β-alumina, *J. Am. Ceram. Soc., 66* (11) (1983) C205–C206.
29 A. K. Chatterjee and G. I. Zhmoidin, The phase equilibrium diagram of the system CaO–Al_2O_3–CaF_2, *J. Mater. Sci., 7* (1) (1972) 93.

4.0 Some Effects of Eutectic Liquid Under Reducing Conditions in the Alumina–Tin Dioxide Composite System

To be published in the *Journal of the American Ceramic Society*

Some Effects of Eutectic Liquid under Reducing Conditions in the Alumina-Tin Dioxide Composite System*

Peter E. D. Morgan# and Robert M. Housley,

Rockwell Science Center, 1049 Camino Dos Rios, Thousand Oaks, CA 91360

Tin dioxide (SnO_2, cassiterite) is one of the few simple oxides that does not react with alumina below an eutectic at 1620°C in air [1]. Consequently it has been of interest for weak interfacial coatings on alumina for ceramic matrix composites (CMC's) [ref. 2 and refs. therein]. At low oxygen potentials, however, the eutectic temperature is significantly reduced to 1045°C, whereupon an oxide liquid, which bears some resemblance to those encountered in the Ag-HTSC (high temperature superconductor) systems, is formed and readily attacks the alumina.**

I. Introduction

The Sn-SnO_2 phase diagram has been determined [3]. On the SnO_2 rich side, as Sn is added to SnO_2 (fixing the oxygen potential at the Sn/SnO_2 buffer) and the temperature is raised, liquid tin, MP 231°C, and SnO_2 coexist up to 1045°C. Above 1045°C a new liquid forms that initially contains ~50.3% Sn and ~49.7% SnO_2; this liquid, dissolving more Sn or SnO_2 as temperature rises, coexists with

---

* and with an unusual connection to liquids present in the Ag-HTSC systems.

Fellow Am. Ceram. Soc..

** other notable ones are ZrO_2, HfO_2 and ThO_2

solid SnO_2 up to the latter's melting point at 1630°C in air. Oxide melts that dissolve a metal (conversely precipitating a metal on cooling) are not common; another trendy, but often misunderstood, example is the temperature reversible solution of Ag metal in the various HTSC eutectic/peritectic melts [e.g., ref. 4 and references therein].

While Al_2O_3 does not react with SnO_2 below the eutectic at 1620°C, it does readily dissolve in the much lower temperature Sn-SnO_2 eutectic liquid; for example, to the extent of ~3.7% at 1360°C [5]. Such dissolution could occur in an Al_2O_3-SnO_2 composite in a reducing atmosphere below the oxygen potential at the Sn-SnO_2 buffer or, indeed, slightly above due to the entropic contribution of the solution of Al_2O_3 in the melt. Above ~300°C the oxygen potential at the Sn-SnO_2 buffer lies above that of the $2CO + O_2 <--> 2CO_2$ buffer [6]. This allows us an easy test of the effects of a reducing environment by exposing an Al_2O_3-SnO_2 composite to a partial CO atmosphere at elevated temperature.

II. Experimental

An ~1cm layer of alumina was placed in a 4.8cm diameter graphite die. An ~1cm layer of SnO_2 powder was next centrally laid with a diameter of ~2.4cm. The SnO_2 was then surrounded by alumina powder and covered over with more alumina powder to a depth of ~2.4cm. This produced a compact with SnO_2 entirely surrounded by Al_2O_3 with a thickness initially of at least 1.2cm. This assembly was hot pressed (HP) in graphite nominally under a nitrogen atmosphere to 1400°C for 1hr at ~2000psi. After the shrinkage due to HP, the central tin-containing region was surrounded by ~1.2cm of Al_2O_3 in all directions. The sample was cut along a diameter and polished.

III. Result and Discussion

The optical micrograph, Figure 1, shows the tin materials inside the alumina cavity. Evident reduction of some of the original SnO_2 to Sn has occurred on the left side. Polishing a composite material as hard as alumina on the one hand, and as soft as tin on the other, is not easy, and some pullout of the tin has occurred.

The presence of both Sn and SnO_2 within the cavity, Fig.1, ensures that we were very near the Sn/SnO_2 equilibrium buffer in the center. The stability of the cavity suggests that the alumina reached a dense strong state (as would be expected) before much reduction commenced.

We can assume that residual oxygen and some water were present in the apparatus and the die and more especially in the powder sample. As the temperature was raised the oxygen reacted with the graphite die to produce some CO_2 and CO in the predominant nitrogen atmosphere. Above about 300°C, the partial pressure of oxygen at the $2CO + O_2 <--> 2CO_2$ buffer becomes lower than that at the $Sn + O_2 <--> SnO_2$ buffer [6] so that CO gas will reduce SnO_2 to Sn metal. At 1400°C, the pO_2 of the former buffer is two orders of magnitude lower, at $\sim 10^{-9}$, than the latter one at $\sim 10^{-7}$ (dilution with nitrogen will prorate both to lower without changing the relative values). Evidently there was enough diffusion of CO in and CO_2 out of the cavity and in and out of the porous die and punches to allow the reduction to occur.

Around the cavity is an obvious reaction zone (aureole) caused by liquid(s) seepage into and interaction with the alumina. SEM microscopic analysis and EDS indicated that this liquid was uniform in its reaction with the alumina even though there was a preferential production of tin metal on the left side as shown. Figure 2 illustrates a region typical of the edge of the aureole; the alumina grains where the liquid has percolated are very much larger than outside the region, as

portrayed by the secondary electron image on the left. The remains of the liquid are evident in the back-scatter electron SEM picture, on the right, as elongated relics along the alumina grain boundaries. This is shown at higher magnification in Fig. 3.

The liquid Sn-SnO_2 appears to be highly corrosive (as the earlier work suggested: see ref. 5) promoting massive alumina grain-growth by solution-reprecipitation. Higher magnification views of selected regions, as in Fig. 4, show that the liquid has precipitated Sn metal (initially as a liquid), SnO_2 and Al_2O_3 on cooling, in agreement with the known phase equilibria [5]. To the upper right of Fig. 2 there is an additional feature, a region containing low levels of tin metal but no SnO_2. It appears that at some lower temperature, when only tin metal was liquid, some of this liquid percolated outwards. As might be expected, liquid tin itself did not encourage grain-growth, presumably because alumina is not soluble in it.

IV. Conclusions

Composites containing SnO_2 can probably be used safely only well above the $Sn + O_2 <--> SnO_2$ buffer (~10^{-7} pO_2 at 1400°C) [6]. This would disqualify them in applications where pO_2 excursions might occur, but would still allow use in a guaranteed oxidizing environment such as in a glass tank. When allowed to form the Sn metal/SnO_2 eutectic liquid appears to be unusually effective in promoting the solution-reprecipitation grain growth of Al_2O_3 (viz., the liquid is "corrosive") as seemingly is the case with the Ag metal-HTSC liquids [e.g., ref. 4 and references therein]. We believe this to be a characteristic of oxidic liquids containing dissolved "metals".

Another interface for alumina systems, which survives these reducing conditions [7], La-monazite, $LaPO_4$, is under development .

Acknowledgments: We thank the US Office of Naval Research for funding support for this work under contract# N00014-91-C-0157. The tricky polishing of these samples was ably performed by Edward H. Wright.

References

1 V. J. Barczak and R. H. Insley, *"Phase Equilibria in the System Al_2O_3-SnO_2"* J. Am. Ceram. Soc. **45** 144 (1962).

2 P. E. D. Morgan and D. B. Marshall, *"Functional Interfaces for Oxide/Oxide Composites"*, Mat. Sci. Eng. **A162** 15-25 (1993) and references therein.

3 Fig. 6309 in Phase Diagrams for Ceramists, NIST/Am. Ceram. Soc. **VI** Eds. R. R. Roth, J. R. Dennis and H. F. McMurdie, (1987).

4 P. E. D. Morgan, R. M. Housley, and J. J. Ratto, *"Low Level Liquid Droplet Mechanism Allowing Development of Large Platelets of High T_c "Bi-2223" Phase Within a Ceramic,"* Physica C **176** 279-284 (1991).

5 U. Kluxmann and R. Dobner, Metall (Berlin), **34** 821-827 (1980).

6 F. D. Richardson and J. H. E. Jeffes, J. Iron Steel Inst. **160** 261 (1948).

7 D. B. Marshall and P. E. D. Morgan, *"Layered Oxide Composites"*, Am. Ceram. Soc. Bull. **73** 214 (SIII-63-94) (1994).

Figures

Figure 1. Cavity in graphite-die-hot-pressed dense alumina, originally containing SnO_2, which has been reduced in partial CO atmosphere to Sn-SnO_2 eutectic liquid and solid at 1400°C. Optical micrograph, magnification X10.

Figure 2. Magnifiied image (SEM of polished surface) showing edge of liquid phase infiltrated "aureole" region.

Figure 3. Highest magnification of edge of liquid infiltrated region.

Figure 4. Details of frozen eutectic liquid which has precipitated Sn metal, SnO_2 (cassiterite), and alumina.

Cavity in graphite die hot-pressed dense alumina originally containing SnO_2 which has been reduced in CO atmosphere to Sn-SnO_2 liquid and solid at 1400°C

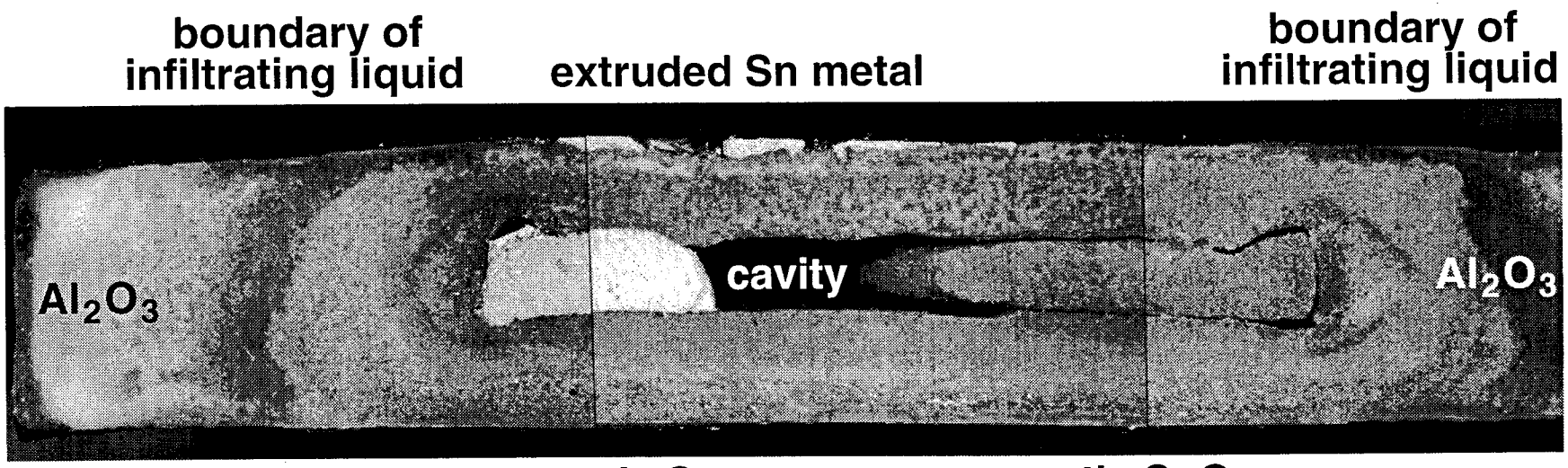

optical micrographs; mag. x10

Fig. 1

Magnified image showing edge of liquid phase infiltration

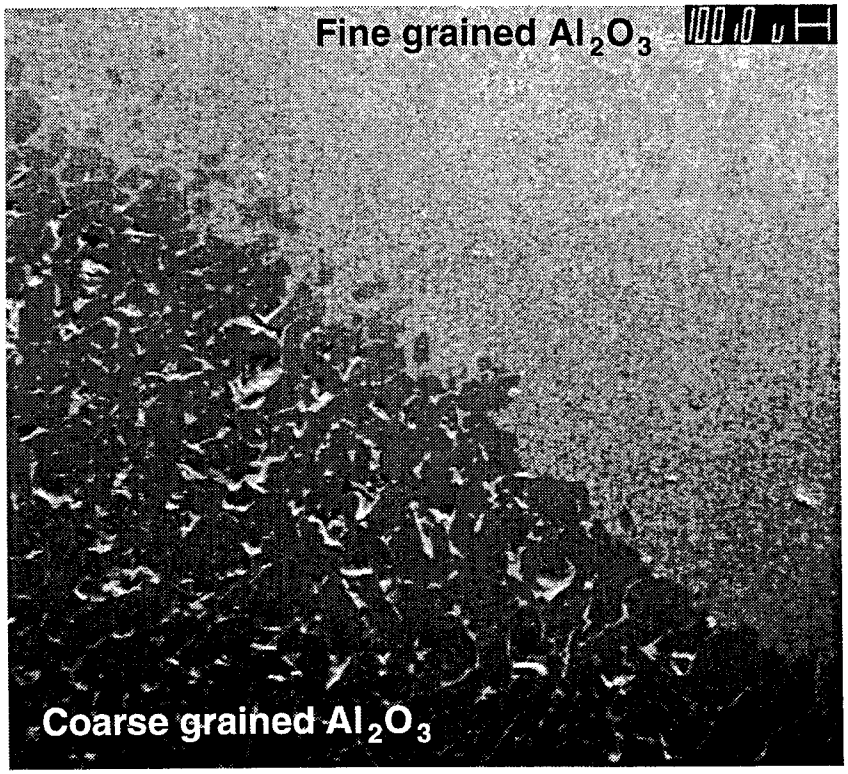

large grain-growth by solution-reprecipitation where liquid infiltrates the alumina, secondary electron image

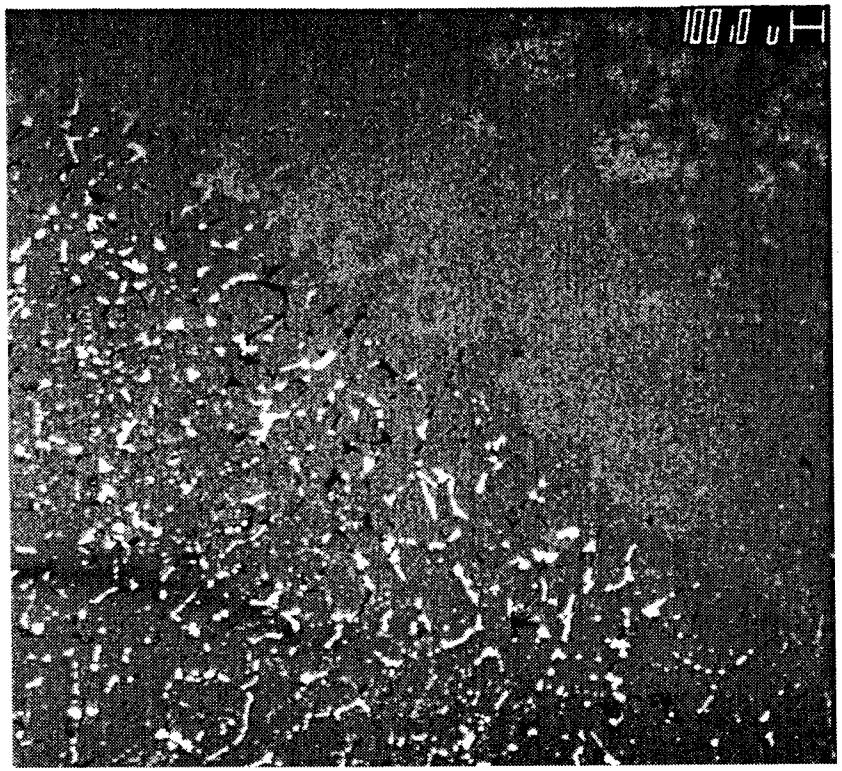

presence of Sn and SnO_2 between the alumina grains shows up lighter by back scatter electron image (BSE)

Fig. 2

Highest magnification of edge of liquid infiltrated area

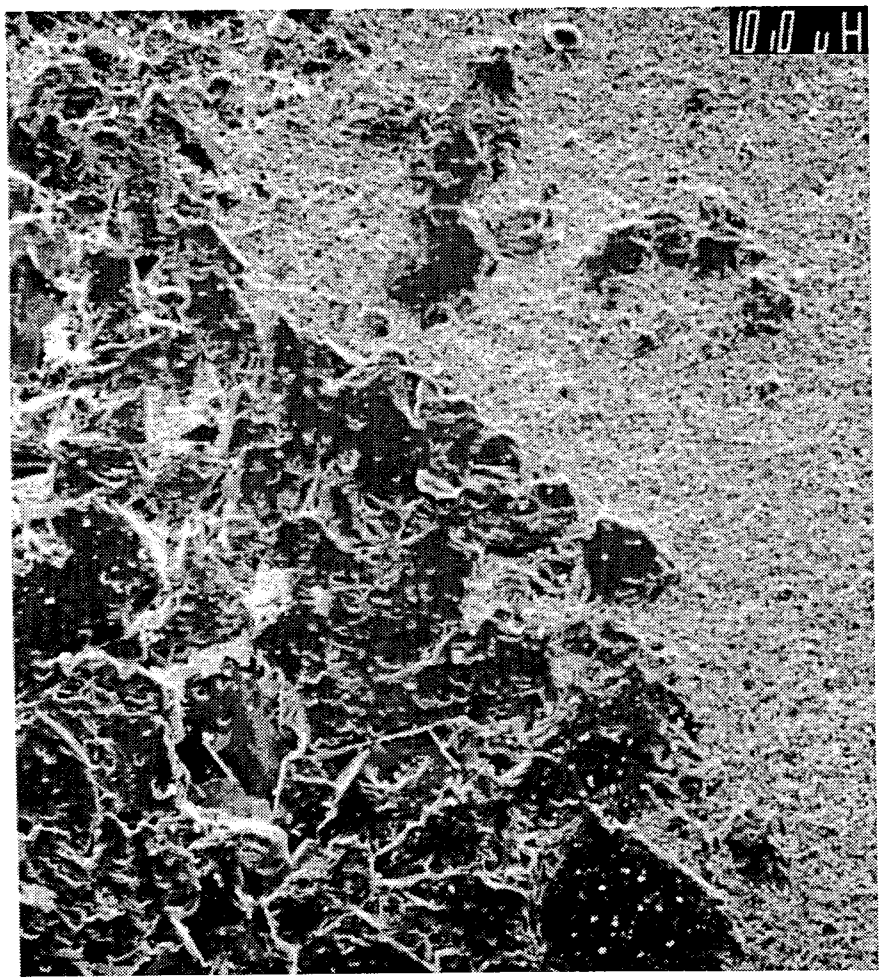

large grain-growth by solution-reprecipitation where liquid infiltrates the alumina, secondary electron image

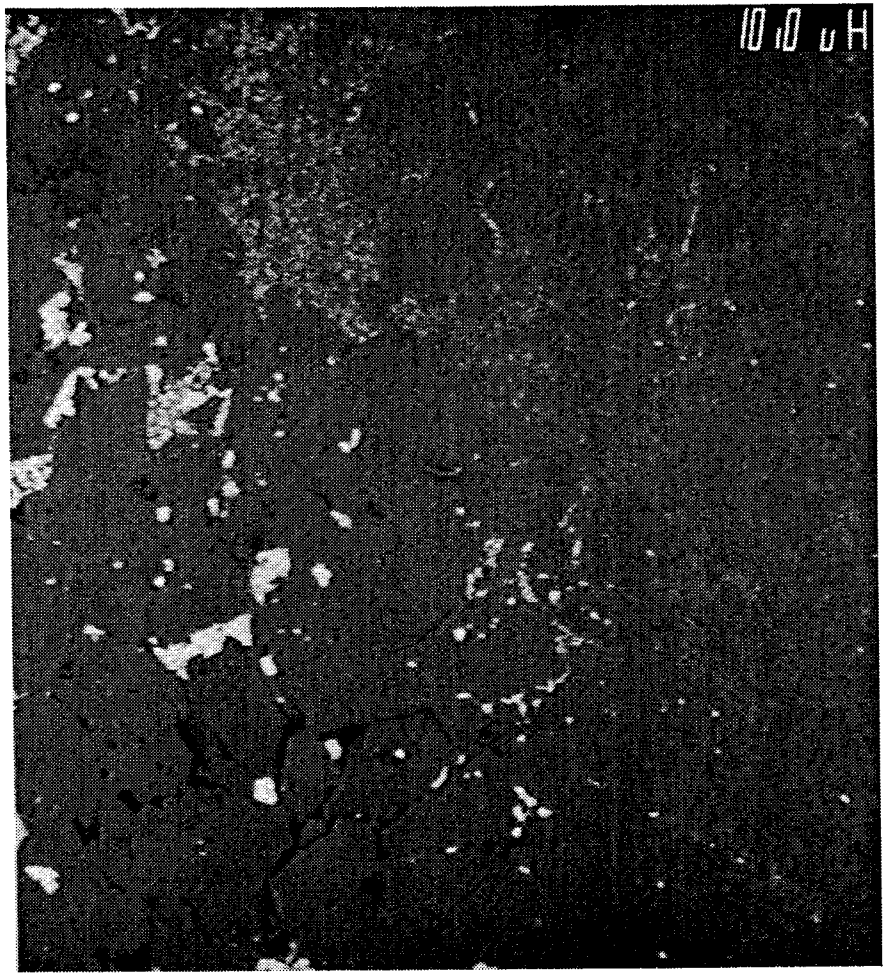

presence of Sn and SnO_2 frozen liquid between the alumina grains shows up lighter by back scatter electron image (BSE)

Fig. 3

Details of frozen eutectic liquid which has precipitated Sn metal, cassiterite and alumina

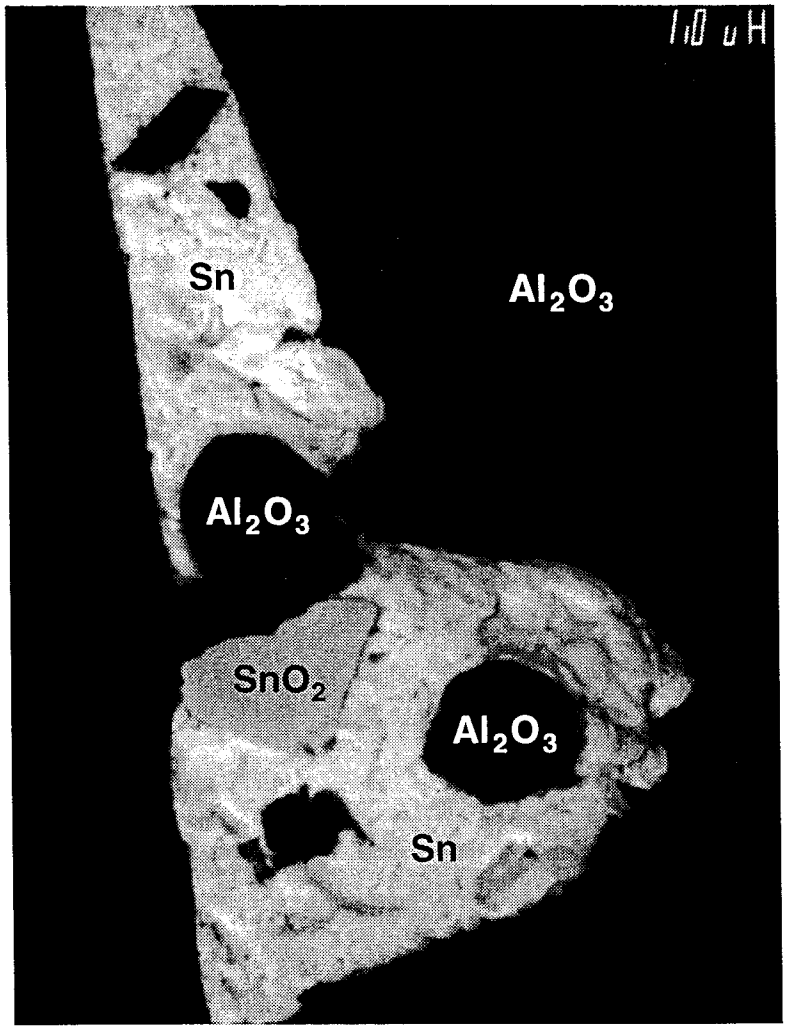

Fig.4

Back scatter electron images of selected frozen liquid areas wherein we see the separate Sn metal (off-white), SnO_2 (cassiterite, gray), and alumina (mostly black) that precipitated from the oxidic eutectic liquid

5.0 Ceramic Composites of Monazite and Alumina for Stability in High Temperature Oxidizing Environments

To be published in the *Journal of the American Ceramic Society*

PP 94-121

Rockwell

Materials Science, Rockwell Science Center

Ceramic Composites of Monazite and Alumina for Stability in High Temperature Oxidizing Environments

Peter Morgan and David Marshall
Rockwell Science Center
1049 Camino Dos Rios
Thousand Oaks, CA 91360

Submitted to *The Journal of the American Ceramic Society,* June 1994

CERAMIC COMPOSITES OF MONAZITE AND ALUMINA FOR STABILITY IN HIGH TEMPERATURE OXIDIZING ENVIRONMENTS

Peter Morgan and David Marshall
Science Center
Rockwell International Corporation
1049 Camino dos Rios
Thousand Oaks, CA 91358

ABSTRACT

A new family of high temperature, oxidation resistant ceramic composites, containing monazite ($LaPO_4$) as a weakly bonded phase is proposed. Monazite is shown to be stable and phase compatible with alumina at temperatures at least as high as 1750°C in air. Most important, for use in high toughness composites, the monazite–alumina interface is shown to be sufficiently weak that interfacial debonding prevents cracks from growing from monazite into alumina. Observations of fracture response of fibrous and laminar reinforcements are presented.

June 1994

for: The Journal of the American Ceramic Society.

1. INTRODUCTION

The uses for existing ceramic composites that rely on carbon or boron nitride fiber coatings to prevent brittle failure are severely limited by the instability of the composites in high temperature oxidizing environments. In an attempt to overcome this limitation, several all oxide composite systems (such as aluminum oxide fibers and matrix) have been explored recently.[1-8] However, suitable oxidation-resistant, weakly bonded interphase materials have yet to be demonstrated.

For a coating on alumina fibers to operate successfully in an alumina matrix composite at high temperature we need: 1) chemical compatibility, 2) morphological compatibility, 3) refractoriness, 4) stability in oxidizing and preferably also in, at least, slightly reducing atmosphere, 5) stability in water vapor and carbon dioxide environments and, perhaps, other even more corrosive situations and 6) weak interfaces capable of debonding. This is an extremely demanding set of requirements and, with the choices being limited by the availability of elements in the periodic table, the odds are long that any answer exists at all!

Alumina is an amphoteric oxide (exhibiting both basic and acidic properties) and so is phase compatible (viz., does not chemically react) with only a few simple oxides. It readily reacts with either acidic or basic oxides, ruling out all simple oxides of elements on the left- or right-hand sides of the conventional periodic table, leaving only a few oxides of elements towards the center of the table, and especially lower down, such as SnO_2, ZrO_2 (and HfO_2), TiO_2 (below 1420°C) and a few others which either are not sufficiently refractory (e.g., In_2O_3), or are impractical (ThO_2), or which are easily reduced to metal. We have earlier discussed the potential use of the compatible mixed aluminates, such as the β-alumina/magnetoplumbite family,[1] which have since attracted the attention of other workers.[2,9]

Another set of choices potentially exists, however, in the mixed oxides, especially where an element from the left-hand side of the periodic table (basic) and an element from the right-hand side (acidic) form a neutral mixed oxide, or rarely other compound types (e.g., CaF_2 or LaF_3). Typical prospects would be $BaSO_4$ (barite), $LaPO_4$ ((La)-monazite), and perhaps a few others such as $CaTiO_3$ perovskite, all well-known in natural mineral assemblages with alumina (in particular Ref. 10). We confirmed earlier that $CaTiO_3$ is phase compatible with alumina[11] (they also occur together as early solar system relics in carbonaceous chondrite meteorites). Most other similar mixed oxides would not be sufficiently refractory, or would be either too strong in themselves or tending to bond too strongly to alumina. Because a compound is compatible it does not follow that it forms weak interfaces (cf. alumina and zirconia). We recognize too that, as the number of elements involved in matrix and interface increase, so does the chance of undesirable lower melting eutectics (or peritectics).

During our preliminary scoping tests,[1] it rapidly became apparent that (La)-monazite (hereinafter referred to simply as monazite) was in a class of its own in terms of its favorable physical properties and interface properties with alumina. Monazite is non-toxic being completely insoluble in water and dilute acids and bases; (surprisingly?) refractory, MP 2072 ± 20°C [6] (which is higher than alumina!) with no decomposition up to the melting point; and not easily reduced–it survives hot pressing in graphite to 1400°C (oxygen partial pressure ~10^{-9}atm), when not in direct contact with the solid graphite, which SnO_2 does not.[13]

$LaPO_4$ is monoclinic, (a=6.825Å, b=7.057Å, c=6.482Å, β=103.21°) with four formula units in the $P2_1/n$ (14) unit cell.[14] It belongs to a large structural family (e.g. Ref. 15, 16) which includes chromates vanadates, celenates and other phosphates. Phosphorus is 4-coordinated in a distorted tetrahedral environment; La is nine-coordinated by O in an unusual arrangement while O is 3- or 4-coordinated to 2 or 3 La and 1 P.[14] The density of $LaPO_4$ is 5.13 g/cc.

Monazite is a well–known, commercially important mineral which contains mixed (larger) rare earths and usually thorium and uranium often at quite high levels. It occurs

commonly in the acidic granites (and their pegmatites), which ensures that it is compatible with a wide range of silicate minerals such as quartz, felspar, micas, amphiboles, garnets, zircon, titanite (sphene), and cassiterite and fluorite. In a large variety of other pegmatites, e.g., in gneissic and syenitic rocks, it is compatible with silimanite, andalusite and kyanite (and therefore probably mullite) sapphire, spinel, rutile (anatase), gadolinite, and many others. In the more unusual alkalic carbonatites it is compatible with perovskites, pyrochlores, apatite, zirconolites, baddeleyite, fergusonites, xenotime, calcite, barite, celestine, bastnaesite and many more. In the mafic (basic) basalts, monazite does not occur; in the rare cases of close association with such rocks,[17,18] alteration appears to have occurred. In these the monazite is additionally phase compatible with olivine and pyroxenes. Indeed, probably hundreds of minerals are known to be phase compatible with monazite. It reacts less with water than almost all minerals; it is consequently found also as a resistate in placer deposits and beach sands, while in alluvial deposits there is evidence that individual monazite grains (like zircon) can survive several cycles of weathering and reconsolidation; this augurs well for high temperature stability against stress corrosion in the humid atmosphere of combustion gases.

Although nature has performed innumerable phase stability experiments, only recently have a few studies of monazite phase diagrams been done by humans.[19,21] "Phase Diagrams for Ceramists"[22] contains no diagrams involving monazite, part of a dearth of diagrams for rare earth oxide systems in general; this seems a curious oversight for such refractory materials with possible uses. Its potential use as a radioactive waste host or encapsulant,[23] on account of its water insolubility, has not, however, escaped attention; this reference is also an extensive and useful review of monazites.

2. EXPERIMENTAL

2.1 Fabrication of Test Specimens

The following raw materials were used to fabricate a variety of test specimens: single crystal alumina fibers from Saphikon, alumina powder from Sumitomo (99.99% α-alumina AKP30), alumina powder from Ceralox (α-alumina containing 0.5 weight % MgO) and hydrated $LaPO_4$ from Stremm Chemical Company. The monazite had been made by precipitation from aqueous solution with potassium phosphate. After discovering that the monazite contained ~1% potassium (and after discussions with the vendor), tests were made to remove the potassium by simple cold water washing: this succeeded in lowering the potassium content to less than 0.3%.

Initially, the compatibility of alumina and monazite was tested by firing powder mixtures in air at temperatures up to 1750°C. X-ray analysis indicated that no reactions occurred. Within the accuracy of present lattice parameter measurements, solid solution of alumina in monazite was not detected. However, since the solubility is not likely to be absolutely zero, all monazite used for fabrication of test specimens was prefired at 1100°C with the addition of 1% by weight of AlOOH (Disperal®) to ensure that any solid solution limit was exceeded, and thus avoid possible reaction with the fibers; in the final microstructures small amounts of Al_2O_3 were always detected as a second phase, confirming that the solid solution limit was indeed exceeded.

Several types of composites were fabricated to allow testing of compatibility, stability, and fracture properties of monazite–alumina interfaces as well as evaluation of some relevant physical properties of bulk monazite itself. One specimen consisted of monazite powder and a few sapphire fibers, hot pressed at 1300°C using graphite dies in a N_2 atmosphere. Test pieces cut from regions without fibers were used for measuring

thermal and mechanical properties of the monazite, while test pieces cut from the region containing fibers were used for interface studies. Other fibrous composites were fabricated by dip-coating up to 200 sapphire fibers in a monazite slurry embedding the coated fibers in Ceralox alumina powder, and hot pressing at 1400°C.

Layered composites of alumina (Sumitomo) and monazite, with layer thicknesses within the range 1 μm and 500 μm, were fabricated by colloidal methods. This involved preparation of separate suspensions of alumina and monazite and consolidation either by sequential centrifuging (as described elsewhere for Al_2O_3-ZrO_2 composites[25]) or by sequential vacuum slip casting. The slurries were prepared by first dispersing the powders at pH2 and then adding NH_4NO_3 to a concentration of 2M to generate strong short-range repulsive forces between particles, as described by Velamakanni et al.[26] After drying, the compacts were either sintered in air (1600°C for 2 hours) or surrounded by dry alumina powder and hot-pressed (1400°C for 1 hour).

2.2 Interface Testing

Several test specimens (Fig. 1) were used for qualitative and quantitative evaluation of interfacial properties. For simple determination of whether or not debonding occurs, a surface was polished normal to the interface and a Vickers indenter was loaded onto the surface near the interface as shown in Fig. 1(a). The radial crack that grew towards the interface was then used to test for debonding or penetration. The sliding resistance of coated fibers was measured by pushout of the fibers from a thin slice (~0.5 mm thickness) of composite using a flat-ended diamond indenter (Fig. 1(b)).[27-30] Quantitative measurements of the interfacial debond energy were obtained for the laminar composites by flexural loading of notched beams that contained layers of monazite in their midsections, as indicated in Fig. 1(c). Loading was applied using an instrumented fixture attached to the stage of an optical microscope, thus allowing crack growth to be observed in situ. After growing from the notch normal to the monazite layers, the cracks

deflected along the layers. The load required to cause debonding along the monazite layer was used with the analysis of Charalambides et al.[31] to evaluate a debond resistance.

3. PROPERTIES OF MONAZITE

3.1 Sintering/Hot Pressing

No reduction of monazite in the hot pressing atmosphere of nominal N_2/graphite at 1400°C was ever observed, although some reaction was observed when monazite directly contacted graphite at 1400°C. In initial tests using as-received monazite, proximity to alumina was found to cause an increase in densification. This originated from the formation of a minor liquid phase which was rich in potassium and contained lanthanum and aluminum (Fig. 2). This liquid apparent in the interstices between the rounded grains especially near the fiber is consistent with the known eutectic in the La-K-P-O system at 840°C.[19-21] This eutectic was largely eliminated by washing the monazite powder to lower the potassium content, as described in the previous section.

3.2 Thermal Expansion Properties

The thermal expansion properties were measured over the temperature range 20°C to 1000°C using a bar cut from a specimen of monazite that was fabricated by hot pressing at 1300°C. The results are shown in Fig. 3. The average coefficient of thermal expansion over this temperature range is $9.6 \times 10^{-6}\,^{\circ}C^{-1}$, approximately 25% higher than that of alumina.

3.3 Elastic Properties

The Young's modulus was measured as 133 GPa by ultrasonic resonance using the same bar that was used for thermal expansion measurement. The bar was then loaded in 4–point flexure with strain gauges attached to its surfaces between the inner loading points; one gauge was on the tensile surface aligned parallel to the direction of the

applied stress, while the other was on the compressive surface aligned normal to the applied stress. The stress strain curve was linear elastic with a Young's modulus of E= 134±1 GPa, agreeing with the resonance measurement. The Poisson's ratio was ν=0.275±0.005.

3.4 Hardness and Toughness

The hardness and fracture toughness of the specimen used for thermal expansion and elastic measurements were measured by Vickers indentation in air, at loads within the range 0.5–100N. Despite some chipping around the indentations, the hardness calculated from the relation $H=P/2a^2$, where P is the indenter load and 2a is the diameter at the contact impression, was constant within the measurement error over this load range (H=5.6±0.4GPa). The fracture toughness calculated from the lengths of the radial cracks, using the analysis of Chantikul et al.,[31] was also constant, $K_c=1.0 \pm 0.1 MPa.m^{1/2}$, over the load range 10 - 100N. At lower loads the cracks were irregular and were not used in the toughness evaluation.

The fracture toughness was also measured by loading a notched beam of the same material in bending. The beam dimensions were 20 × 8 × 1 mm, with a notch depth of 3 mm. The load was applied to the notched beam using a fixture on the stage of an optical microscope, thus allowing in situ observation of the side of the beam during loading. Complete fracture of the beam was observed immediately after initiation of a crack from the notch root, without any precursor stable growth. The toughness calculated using the expression from Tada,[33] with the initial crack length taken equal to the notch depth, is $K_c \approx 1 MPa.m^{1/2}$. Because of the finite notch root radius (~50 μm), this value is expected to be an overestimate. However, given the agreement with the indentation toughness, this error appears to be insignificant. The fracture energy obtained using the relation $\Gamma=K_c^2(1-\nu^2)/E$, with $K_c=1 MPa.m^{1/2}$ and values of E and ν from the preceding section, is $\Gamma=7 J/m^2$.

4. INTERFACIAL DEBONDING

4.1 Indentation Observations

The propensity for interfacial debonding was assessed initially in each composite using the indentation method indicated in Fig. 1(a). In all cases the indentation cracks (both radial and lateral) were deflected at the monazite–alumina interface, as illustrated in Fig. 4 for a monazite layer within an alumina matrix and in Fig. 5 for the composite containing coated sapphire fibers in a polycrystalline alumina matrix. Deflection of subsurface lateral cracks was also confirmed by optical observations in reflection using crossed polars, which removed reflections from the specimen surface but not from subsurface cracks. The role of the monazite coating in promoting the debonding observed in Fig. 5(a) is confirmed in Fig. 5(b), which shows a region of the same composite with an uncoated fiber: in this case, the radial crack passed through the strongly bonded interface into the fiber without deflecting.

More details of the interfacial cracking are evident in the scanning electron micrographs of Fig. 6, in which the monazite coating exhibits atomic number contrast. Cracks generally tended to cross the matrix (alumina)/monazite interface into the coating and deflect along the monazite/fiber (sapphire) interface, as can be seen in Fig. 6(b). A similar behavior is observed in the layered composite in Fig. 4(b). This response is discussed in Section 6, while more detailed observations of the debonded surfaces are given in Section 5. Multiple cracks commonly formed within the monazite layer where the indentation crack entered from the matrix, as in Fig. 6(b).

Whenever the direction of the radial indentation cracking was offset from the center of the fiber, so that the crack deflected around one side of the fiber as in Figs. 5 and 6, a second crack also formed along the fiber–monazite interface on the opposite side of the fiber. The second crack was not connected to the indentation crack (at least on the

specimen surface) and was apparently induced by the residual tensile hoop stress associated with the indentation. (Such interfacial cracking was also observed when the indentation was rotated by 45° relative to the position shown in Fig. 1(a), so that neither of the radial cracks intersected the fiber.)

The residual hoop, stress σ_t, due to a Vickers indentation can be expressed as[34]

$$\sigma_t/H = \eta(a/r)^3 \tag{1}$$

where H is the hardness (of alumina), 2a is the diameter of the indentation, r is the distance from the center of the center of the indentation, and η is a function of the ratio of the size of the indentation to the radius of the plastic zone surrounding the indentation. For alumina, the analysis of Ref. 34 gives $\eta = 0.12$. With the measured hardness H = 20 GPa for the alumina matrix, and with the observation that debonding typically occurred for indentations closer than $r \approx 3a$, Eq. (1) gives a strength of ~ 200 MPa for the monazite–alumina interface.

4.2 Fiber Pushout

The fiber push test of Fig. 1(b) was used to test the ability of the coated fibers to debond and slide under axial loading, as required for toughening of a fiber reinforced composite. Sliding was observed with a load of 10 N on fibers in a slice of 0.46 mm thickness: the end of the fiber that was pushed out of the backside of the slice in one such experiment is shown in Fig. 7. The average shear stress τ_{av} along the interface at the onset of sliding is[27]

$$\tau_{av} = F/2\pi Rd \tag{2}$$

where F is the applied load, R is the fiber radius, and d is the thickness of the slice. With the above mentioned data and the fiber radius R = 40 μm, we obtain τ_{av} = 85 MPa. The

experiment does not distinguish the possible separate contributions due to interfacial debonding energy and frictional sliding resistance over the debonded interface.

4.3 Fracture of Layered Composites

4.3.1 Composites Containing Isolated Monazite Layers

Beams of laminar composites containing several widely spaced layers of monazite were fractured by loading in 4–point bending, as in Fig. 1(b). The beam dimensions were ~ 50 × 10 × 2 mm, with notch depth 1 mm and load points separated by 40 mm and 4 mm. The monazite layer thicknesses were ~10 to 50 μm. Extensive delamination occurred along the monazite layers, as shown in Fig.8.

In situ observations revealed that the crack initiated from the base of the notch and grew to the first layer, where the crack arrested and caused the layer to delaminate (Fig. 8(a)). Then the load was increased by a factor of more than two before a new crack initiated in the next alumina layer and grew unstably across the remainder of the specimen. This rapidly growing unstable crack also caused delamination at the other monazite layers and separate reinitiation in the alumina layers Fig. 8(c).

Two different fracture processes were observed during delamination of these layered composites. In several cases delamination occurred along the monazite–alumina interface, as in the sapphire reinforced composite. More commonly, after the initial crack arrested at the monazite-alumina interface, further delamination began with the initiation of an array of sigmoidal microcracks within the monazite layer. The microcracks were oriented at ~40° to the layers (approximately normal to the local tensile stress), as shown in the in situ optical micrograph of Fig. 9 (a). (The cracks were made visible using internally scattered light: the field limiting aperture of the microscope was reduced in size to illuminate only a small area and the cracks were placed outside the directly illuminated area.[35] The cracks were not visible in direct illumination or if the specimen was

unloaded.) With continued loading the array of microcracks spread and those closest to the initial precrack linked together, leading to the well developed configuration depicted in Fig. 9(c), consisting of a damage zone of microcracks (or cohesive zone) ahead of a continuous delamination.

The delamination resistance Γ_{ss} was evaluated using the analysis of Charalambides et al.:[31]

$$\frac{\Gamma_{ss} E b^2 h^3}{P^2 \ell^2 (1-\nu^2)} = f\left(\frac{h_1}{h_2}, \frac{E}{E_1}\right) \tag{3}$$

where f is a function defined in Ref. 31, P is the load needed to cause debonding, E and E_1 are the Young's moduli of the materials above and below the delamination, and the other parameters are specimen dimensions defined in Fig 1(a). The test pieces used for these measurements contained only a few layers of monazite with thicknesses much smaller than the width of the beam. Therefore, the values of E and E_1 were taken to be equal to the Young's modulus of alumina. The steady-state condition required for Eq. (1) is satisfied when the length of the delamination crack, a, is larger than the thickness, h_1, of the upper layer. Then, if G_{ss} is independent of crack length, the load required to extend the crack is also independent of a.

In the monazite–alumina composites such as that in Fig. 9, the delamination (as measured from the leading edge of the microcrack zone) grew stably with increasing load, indicating that the delamination resistance increases with increasing crack length, as indicated in Fig. 10. The increasing delamination resistance is associated with the evolution of the zone of partially cracked material prior to achieving the well developed configuration of Fig. 9(c).

A rigorous evaluation of the intrinsic fracture energy of the monazite–alumina interface from these experiments would require analysis of data from the initial stages of

delamination, where the cracks grow along the interface and where nonsteady state solutions apply. Nevertheless, a reasonable approximation to the initial delamination resistance may be obtained by extrapolating the data in Fig. 10 to zero crack length. The calculated strain energy release rate for the interface crack would also be affected by the lower elastic modulus of the thin sandwich layer of monazite. Suo and Hutchinson[36] found that the lower modulus of the thin layer can be accounted for by a multiplying factor of $(1-\alpha)$, where α is an elastic mismatch parameter given by

$$\alpha = \left(E_2' - E_1'\right) / \left(E_2' + E_1'\right) \tag{4}$$

where $E' = E/(1-\nu^2)$ and the subscripts 1 and 2 refer to monazite and alumina. With $E_2 = 400$ GPa for alumina and $E_1 = 133$ GPa for monazite (Section 3.3), Eq. (4) gives $\alpha = 0.5$. The extrapolated value from Fig. 8 modified by this factor yields an estimate of $\sim 2.5\ J/m^2$ for the interfacial debond energy.

The cracking mechanism shown in Fig. 9 is very similar to cracking observed under shear loading in unidirectionally reinforced glass matrix composites,[37,38] in brittle adhesive joints between rigid layers loaded in shear,[39] and in delamination of graphite epoxy systems.[40,41] Xia and Hutchinson[42] recently developed a cohesive zone model for this fracture mechanism, which predicts that the steady-state macroscopic mode II fracture energy is larger by a factor of 3 to 4 than the mode I fracture energy of the layer. The data in Fig. 10 at large crack lengths appear to be approaching a steady state value that is approximately double the measured fracture energy of monazite. Given that the loading in these experiments is not pure mode II (the phase angle is approximately 50°) the results are qualitatively consistent with the analysis of Xia and Hutchinson.

4.3.2 Multilayered Composites

Several composites containing up to several hundred layers of monazite and alumina with thicknesses in the range 10 μm to 100 μm were fabricated. In these

composites, the delamination response was variable: delamination generally occurred within the thicker layers; but at many of the thinner layers, no obvious delamination occurred. In specimens that did not delaminate, in situ observations revealed that extension of the main crack involved crack initiation in the alumina layers ahead of the main crack and linking of these back to the main crack through the monazite layers (Fig-11), a sequence that is reminiscent of the behavior of metal–ceramic layered composites.[43]

The crack initiation process in the alumina layers ahead of the crack tip must be dictated by flaws within the layers. In these composites, no attempt was made to control the grain size within the alumina layers, so that the grain size was relatively large (~5-10-μm), and the strength of the alumina layers would be low. Therefore, increasing the strength of the alumina layers by controlling their grain size would be expected to inhibit crack initiation ahead of a main crack and thus promote delamination.

4.3.3 Hybrid Composites: Crack Bridging By Sapphire Fibers

A layered alumina–monazite composite containing sapphire fibers within a thick monazite layer conveniently demonstrated that fibers can debond and pull out between the faces of a crack. In a notched beam of this composite, the crack penetrated the monazite layer without breaking the sapphire fibers and delaminated along the monazite–alumina interface, as indicated in Fig. 12. As loading continued, in situ observations revealed that the end of the fiber where it met the polished side face (see Fig. 12(a)) was pulled below the surface (Fig. 12(b)). This observation provides direct evidence that sapphire fibers in a monazite matrix can provide crack bridging by debonding and pullout.

5. INTERFACIAL MORPHOLOGY

The morphology of the interface between the monazite coating and the sapphire fibers was revealed by fracturing a beam of the composite containing coated fibers as illustrated in Fig. 13(a). The micrographs in Figs. 13(b) and 13(c) from matching areas of the exposed surfaces show that separation occurred very cleanly along the sapphire–monazite interface. Where monazite grain boundaries intersected the fiber, surface diffusion had formed ridges on the fiber and corresponding cusps in the monazite (Fig-11(d)). Similar features were replicated on the surface of the fiber that was exposed by pushout (Fig. 7), indicating that debonding and sliding occurred cleanly along the interface in that case as well. Apart from the grain boundary ridges, there was no apparent damage to the fiber from the presence of the monazite. Similar observations were found for the surface of the fiber exposed by pullout in Fig. 12.

6. DISCUSSION

Whether or not a crack approaching an interface between two materials will debond along the interface rather than penetrate into the second material depends on the ratio Γ_i/Γ_2 of the fracture energies of the interface and the second material. The critical values of Γ_i/Γ_2 calculated by He and Hutchinson[44] are shown in Fig. 14(a), plotted as a function of the elastic mismatch parameter α defined in Eq. (4). For a crack growing from monazite to alumina, the following parameters are obtained: α = +0.5 (Sect. 4.3.1), $\Gamma_i = 2.5\ J/m^2$ from Section 5.3, and $\Gamma_2 = 20\ J/m^2$ for Al_2O_3. In this case the value of Γ_i/Γ_2 falls below the critical value in Fig. 14, so that debonding would be expected as observed in Section 4.

For a crack growing in the reverse direction, from alumina to monazite, a different response is predicted. In that case, Γ_2 is the fracture energy of monazite (~7 J/m^2 from Sect. 3) and the sign of α is changed, corresponding to interchanging the two materials.

The corresponding value of Γ_i / Γ_2 (0.35) falls above the critical condition, where the crack is predicted to grow into the monazite. This response is consistent with the observations of Section 4.

The fracture energies calculated in the previous sections are qualitatively consistent with relative surface energies that would be deduced from observed dihedral angles. Observations of thermally etched surfaces such as Fig. 4(b) indicate that the depth of grain boundary grooving increases (and cohesive energy decreases) in the following order: alumina–alumina; monazite–monazite; and monazite–alumina. This ranking is also consistent with the shapes of the triple junctions formed where monazite grain boundaries meet the surface of a sapphire fiber (Figs. 6,7 and 13). The angles of the ridges formed on the sapphire fibers are close to 180°, indicating that the interfacial energy for monazite–alumina is much higher than the monazite–monazite grain boundary energy, thus implying that the cohesive energy of the monazite–alumina interface is smaller. Similar ridges were observed by Davis et al.[45] on sapphire fibers that had been coated with molybedenum, heat treated at 1400°C, then etched to remove the coating. A substantial reduction in fiber strength was also observed. However, the ridges in that case appeared to be sharper and were associated with breakup of the polycrystalline Mo coating. The monazite coatings and layers in the present study did not break up in this manner, even after extended heat treatments at 1600°C. The coating stability would be enhanced by the large interfacial energy (and hence large dihedral angle) of the monazite–alumina interface

The ridges on the fiber surface are not expected to degrade the strength seriously. The effect of the ridges may be estimated by approximating the surface shapes between the ridges as semielliptical depressions, which would give a stress concentration factor (1-+ 2c/b) where c and b are the depth and width of the depression. With c ~ 0.1 μm and b-~ 5 μm, from Fig. 11, the stress concentration factor is only 1.04.

The question naturally arises as to why monazite bonds so weakly to alumina. We may offer only qualitative conjectures. Firstly, inspection of a model of the monazite crystal structure indicates that it has very open irregular oxygen crystal planes, which have no readily apparent epitaxial relationship with those of the nearly close packed oxygens of alumina; interfaces with good fits seem to be ruled out.

Secondly, we may resort to a (novel ?) use of Pauling's second crystal rule. In the bulk all the oxygens in monazite are bonded to 1 phosphorus and 2 or 3 lanthanums. Because of their higher polarizability, which can reduce the surface free energy, we speculate that oxygens are likely to terminate the surface, remaining bonded to the 1 phosphorus with a bond valence of 5/4 (valence of phosphorus divided by coordination). With likely attachment also to at least 1 lanthanum, a further bond valence of 3/9 is contributed. This adds up to 1.58, a substantial portion of the desired valence bond of 2. In reality bonds near the surface would shorten to increase the valence bond further and attachment to another lanthanum, which sometimes appears possible from the crystal structure, would essentially satisfy the oxygen requirement.

In short, the conjecture is that the low interfacial bonding may be related to the particular crystal structure and the presence of the high valent ion, P^{5+}, with a low coordination of 4, which alone can satisfy a large portion of the valence bond to surface oxygen, leading to weak bonding across the interface to alumina.

7. CONCLUSIONS

The monazite–alumina interface has a sufficiently low fracture resistance to satisfy the condition for interfacial debonding when a crack grows from monazite to alumina. Therefore, monazite is a suitable interphase material for alumina composites. Debonding has been observed in several composite reinforcement configurations: fibers, layers, single crystals, polycrystals. The alumina–monazite system is stable at high temperatures in both reducing (e.g., oxygen partial pressure ~10^{-9} atm at 1400°C) and oxidizing environments; composites were

fabricated both by sintering in air at 1600° C and by hot-pressing in graphite at 1400°C. Results of additional heat treatment experiments that show stability and retention of debonding characteristics after long periods in air at 1600°C will be reported separately.[46]

ACKNOWLEDGMENTS

Funding for this work was supplied by the U.S. Office of Naval Research (Dr. S. Fishman) under Contract N00014-91-C-0157. The authors are grateful to Mr. E. Wright for assistance with specimen preparation, to Dr. R.M. Housley for related microscopy and helpful discussions, and to Mr. M. Cunningham for measurement of the thermal expansion properties of the monazite and the acoustic measurement of the Young's modulus of the monazite.

REFERENCES

1. P.E.D. Morgan and D.B. Marshall, "Functional Interfaces for Oxide/Oxide Composites" *Mat. Sci. Eng.* **A162,** 15-25 (1993).

2. M.K. Cinibulk "β–Alumina-Magnetoplumbite Compounds as Fiber Coatings for Oxide-Oxide Composites" Proc. 18th Ann. Conf. & Exp. on Composites & Advanced Ceramics, Abstr. C-123-94F, *Am. Ceram. Soc.* Bull. **72** 122 (1993).

3. J.B. Davis, J.P.A. Lofvander, A.G. Evans, E. Bischoff and M.L. Emiliani, "Fiber Coating Concepts for Brittle Matrix Composites," *J. Am. Ceram. Soc.* **76** [5] 249-57 (1993).

4. A. Maheshwari, K.K. Chawla and T.A. Michalske, "Behavior of Interface in Alumina/glass Composite," *Mater. Sci. Eng.* **A107** 269-76 (1989).

5. R. Venkatesh and K.K. Chawla, "Effect of Interfacial Roughness on Fiber Pullout in Alumina/SnO_2/glass Composites," *J. Mat. Sci.* Lett. **11** 650-652 (1992)

6. M.H. Jasowiak, J.I. Eldridge, J.B. Hurst and J.A. Setlock, "Interfacial Coatings for Sapphire/Al_2O_3," in *High Temp Review 1991* NASA Conference Publication 10082 (1991) p. 84.

7. R.F. Cooper and P.C. Hall, "Reactions Between Synthetic Mica and Simple Oxide Compounds with Application to Oxidation-Resistant Ceramic Composite," *J. Am. Ceram. Soc.* **76** [5] 1265-73 (1993).

8. W.C. Tu, F.F. Lange and A.G. Evans, "A Novel, Damage-Tolerant Ceramic Composite (Synthetic High Temperature Wood)." Submitted to J.Am.Ceram.Soc.

9. P.W. Brown, "MOCVD of Beta-Alumina" Proc. 18th Ann. Conf. & Exp. on Composites & Advanced Ceramics, Abstr. C-124-94F, *Am. Ceram. Soc. Bull.* **72** 122 (1993).

10. M.L. Dele, P. Dhamelincourt and H.J. Schubnel, "Application of a Raman Laser Microprobe for Determining Inclusions in Various Gems" Samotsvety. Mater. S'ezda NMA, Ed. A.V. Sidorenko, pp 5-17, (1980). (Inclusions of monazite within sapphire gems).

11. P.E.D. Morgan and M.S. Koutsoutis, "Phase Relations in the Ca Ti-Al-O System; Further Studies on Members of the CTA Family" *J. Mat. Sci. Lett.* 4, 321-3 (1985), and erratum ibid. **5**, 122-124 (1986).

12. Y. Hikichi and T. Nomura, "Melting Temperatures of Monazite and Xenotime", *J. Am. Ceram. Soc.* **70**, C-252-C-253 (1987). (MP of monazite--2072 ± 20°C--no decomposition up to the MP).

13. P.E.D. Morgan and R.M. Housley, "Some Effects of Eutectic Liquid Under Reducing Conditions in the Alumina Tin Dioxide Composite System " submitted to *J.Am. Ceram. Soc.*

14. D.F. Mullica, W.O. Milligan, D.A. Grossie, G.W. Beall and L.A. Boatner,"Ninefold Coordination in $LaPO_4$-Pentagonal Interpenetrating Tetrahedral Polyhedron" *Inorg. Chim. Acta* **95** 231-236 (1984).

15. O. Muller and R. Roy, *The Major Ternary Structural Families*, Springer-Verlag, New York, 1974.

16. H. Effenberger and F. Pertlik, "Four Monazite Type Structures: Comparison of $SrCrO_4$, $SrSeO_4$, $PbCrO_4$ (Crocoite), and $PbSeO_4$ ", *Zeit. Krist.* 176 75-83 (1986).

17. A.N. Plasenko, S.M. Frolov and L.I. Polezhayeva, "Genesis of Monazite from Mafic Rocks", *Dokl. Akad. Nauk. SSSR* **264** 153-156 (English transl.) (1984).

18. B.L. Jolliff, "A Monazite Bearing Clast in Apollo 17 Melt Breccia", *Proc. Lunar & Planetary Sci.* **24** 725-6 (1993).

19. W. Jungowska and T. Znamierowska, "Phase Equilibria in a Portion of the System La_2O_3-K_2O-P_2O_5 Rich in P_2O_5" *Mat. Chem. & Phys.* **24** 487-494 (1990).

20. W. Jungowska and T. Znamierowska, "The System $LaPO_4$-KPO_3-$La(PO_3)_3$" *Mat. Chem. & Phys.* **27** 109-116 (1991).

21. W. Jungowska and T.Znamierowska, "The System $LaPO_4$-$K_4P_2O_7$-KPO_3", *J. Thermal Anal.* 39 715-720 (1993).

22. Phase Diagrams for Ceramists, publ. by *NIST/Am. Ceram. Soc.*

23. L.A. Boatner and B.C. Sales, "Monazite", chapter 8, pp. 495-563 in *Radioactive Waste Forms for the Future,* Eds W. Lutze and R.C. Ewing, North-Holland, New York 1988.

24. V.J. Barczak and R.H. Insley,"Phase Equilibria in the System Al_2O_3-SnO_2", *J. Am. Ceram. Soc.* **45** 144 (1962).

25. D.B. Marshall, J.J. Ratto, and F.F. Lange, "Enhanced Fracture Toughness in Layered Composites of Ce-ZrO_2 and Al_2O_3," *J.Am. Ceram. Soc.* **74**[12]. 2979-87 (1991).

26. B.V. Velamakanni, J.C. Chang, F.F. Lange, amd D.S. Pearson, "New Method for Efficient Colloidal Particle Packing via Modulation of Repulsive Lubricating Hydration Forces," *Langmair*, **6** [7] 1323 - 1325 (1990).

27. D.B. Marshall, "An Indentation Method for Measuring Matrix-Fiber Frictional Stresses in Ceramic Composites," *J. Amer. Ceram.* Soc. **67**[12], C259-60 (1984).

28. D.B. Marshall and W.C. Oliver, "Measurement of Interfacial Mechanical Properties in Fiber-Reinforced Ceramic Composite," *J. Amer Ceram. Soc.*, **70**[8] 542 - 48 (1987).

29. M.K. Brun and R.N. Singh, "Effect of Thermal Expansion Mismatch and Fiber Coating on the Fiber/Matrix Interfacial Shear Stress in Ceramic Matrix Composites," *Adv. Ceram. Mater.*, **3** 506 - 509 (1988).

30. P.D. Jero, T.A. Parthasarathy and R.J. Kerans, "Interface Properties and Their Measurement with Fiber Pushout Tests," in *High Temperature Ceramic Matrix Composites*, Ed. R. Naslain, J. Lamon and D. Doumeingts, Goodhead Publishers Ltd., Cambridge, pp. 401 - 412 (1993).

31. P.G. Charalambides, J. Lund, A.G. Evans and R.M. McMeeking, "A Test Specimen for Determining the Fracture Resistance of Bimaterial Interfaces," *J. Appl. Mech.* **56** 77 - 82 (1989)

32. G.R. Anstis, P. Chantikul, B.R. Lawn and D.B. Marshall, "A Critical Evaluation of Indentation Techniques for Measuring Fracture Toughness: 1 Direct Crack Measurements", *J. Am. Ceram.* Soc. **64**[9] 533-538 (1981).

33. H. Tada, P.C. Paris and G.R. Irwin, "*The Stress Analysis of Cracks Handbook.*" Paris Productions, St. Louis, MO (1985).

34. S.S. Chiang, D.B. Marshall, and A.G. Evans, "The Response of Solids to Elastic/Plastic Indentation: I. Stresses and Residual Stresses," *J. Appl. Phys.* 53 [1], 298 (1982).

35. D. Johnson-Walls, D.B. Marshall, A.G. Evans, M.D. Drory, and K.T. Faber, "Evaluation of Reliability of Brittle Components by Thermal Stress Testing," *J. Amer. Ceram. Soc.* 68[7], 363-67 (1985).

36. Z. Suo and J. W. Hutchinson "On Sandwich Test Specimens for Measuring Interface Crack Toughness."

37. A.G. Evans, M.D. Thouless, D.P. Johnson-Walls, E.Y. Luh and D.B. Marshall "Some Structural Properties of Ceramic Matrix Fiber Composites," pp 543-553, proc. Fifth International Conference on Composite Materials ICCM-V, Ed. W.C. Harrigan and J Strife, AIME 1985.

38. A.G. Evans, "Engineering Property Requirements for High Performance Ceramics" *Mater. Sci. Eng.* **71** 3-21 (1985).

39. H. Chai, "Shear Fracture" *Int. J. Fracture* **37** 137-159 (1988).

40. M.F. Hibbs and W.L. Bradley "Correlations Between Micromechanical Failure Processes and the Delamination Toughness of Graphite Epoxy Systems" in *Fractography of Modern Engineering Materials,* Ed. J.E. Masters and J. Au. ASTM STP 948 pp 68-97 (1987).

41. B.W. Smith and R.A. Grove "Determination of Crack Propagation Directions in Graphite Epoxy Structures" in *Fractography of Modern Engineering Materials*, Ed. J.E. Masters and J. Au. ASTM STP 948 pp 68-97 (1987).

42. Z.C. Xia and J.W. Hutchinson "Mode II Fracture Toughness of a Brittle Adhesive Layer", *Mech* - 208.

43. M.C. Shaw, D.B. Marshall, M.S. Dadkhah, and A.G. Evans, "Cracking and Damage Mechanisms in Ceramic/Metal Multilayers," *Acta Met.*, **41**[11] 3311-3322 (1993).

44. M.-Y. He and J.W. Hutchinson, "Crack Deflection at an Interface Between Dissimilar Materials," *Int. J. Solids Struct.*, 25 1053 - 1067 (1989).

45. J. B. Davis, J. Yang and A.G. Evans, "Effects of Composite Processing on the Strength of Sapphire Fiber - Reinforced Composites".

46. P.E.D. Morgan, D.B. Marshall and R. Housley,"High TemperatureStability of Monazite–Alumina Composites," submitted to *Mater. Sci. Eng.*

FIGURE CAPTIONS

1. Methods used for testing interface debonding: (a) cracks generated by Vickers indentation; (b) fiber pushing, and (c) delamination of notched beam.

2. Interface between sapphire fiber and monazite matrix which contained potassium impurities.

3. Thermal expansion of monazite.

4. Arrest of indentation crack at monazite layer within alumina matrix: (a) optical micrograph, (b) scanning electron microscope.

5. Optical micrographs showing crack interactions with sapphire fibers in polycrystalline Al_2O_3 matrix: (a) fiber with coating of monazite (b) uncoated fiber.

6. Scanning electron micrograph of fiber as in Fig. 5(a) showing details of monazite coating morphology and cracking.

7. Scanning electron micrograph from bottom of beam of composite (monazite coated sapphire fibers in polycrystalline matrix) after fiber pushout test as in Fig-1(b).

8. Debonding in layered monazite–alumina composite. Notched beam loaded in bending: (a) and (b) cracking of first monazite layer with increasing applied load; (c) after failure of beam.

9. (a) Optical micrograph showing arrays of cracks produced during initial debonding of the first monazite layer in Fig. 8; (b) Schematic showing crack morphology in (a); (c) schematic showing well developed crack.

10. Fracture energy for delamination in specimen from Fig. 9.

11. Schematic showing mechanism of crack advanced in some multilayered alumina–monazite composites with small layer thicknesses.

12. (a) Fracture of multilayer monazite–alumina composite containing sapphire fibers within a thick monazite layer (b) Scanning electron micrograph showing fiber that intersected polished side surface as indicated in (a); depression of fiber below surface is caused by debonding and pullout between crack surfaces.

13. Scanning electron micrographs from debonded surfaces of composite (monazite coated sapphire fiber in polycrystalline matrix) that had been broken as indicated in (a): (b) and (c) are from matching areas of fiber and monazite coating.

14. Schematic showing interface structure between polycrystalline monazite and sapphire and balance between grain boundary and surface energies.

15 Comparison of measured fracture energies with the debonding criterion of He and Hutchinson.[43]

(a)

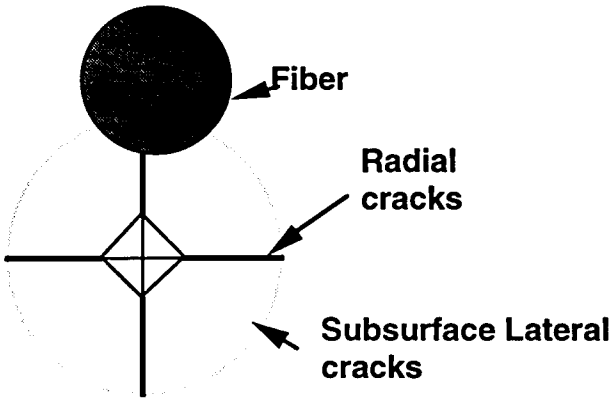
Fiber
Radial cracks
Subsurface Lateral cracks

(b)

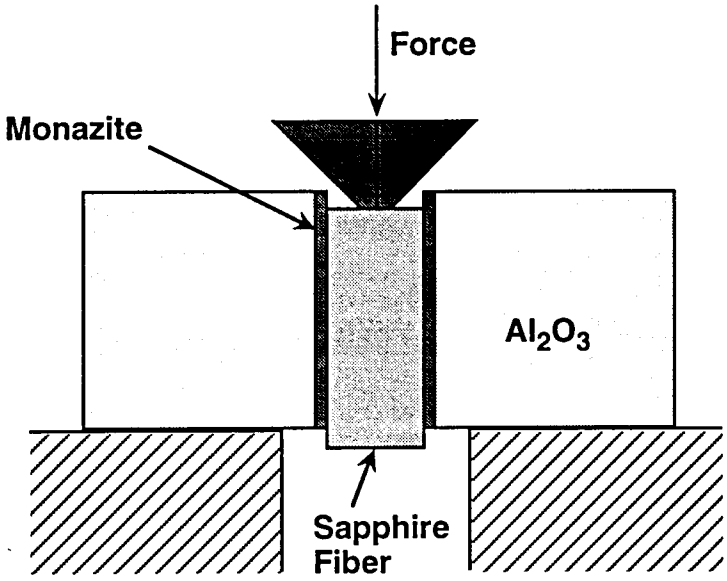
Force
Monazite
Al_2O_3
Sapphire Fiber

(c)

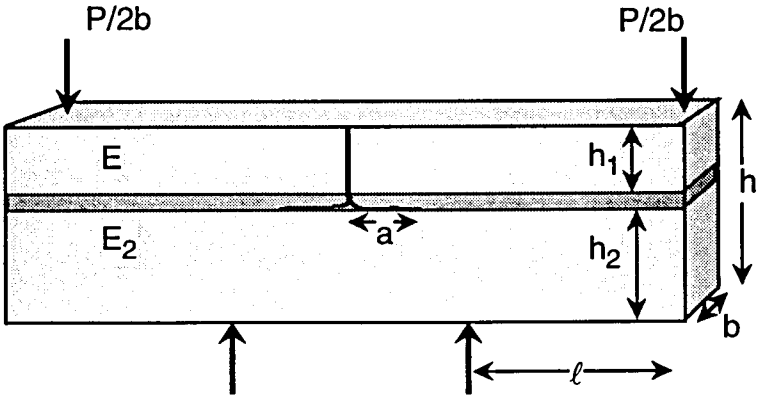
P/2b
P/2b
E
E_2
h_1
h_2
h
a
b
ℓ

Fig. 1

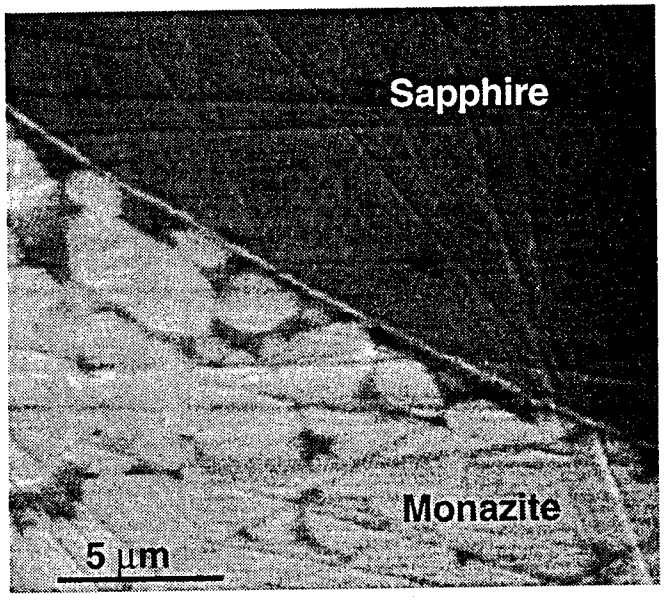

Fig. 2

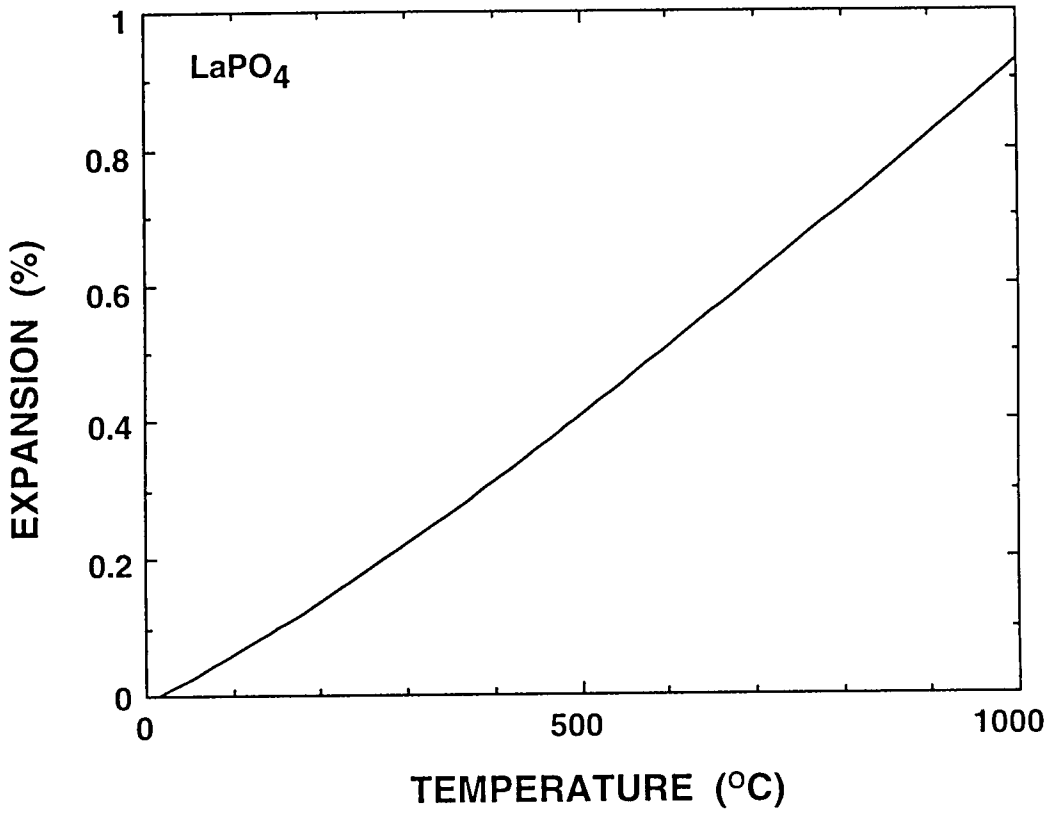

FIG. 3

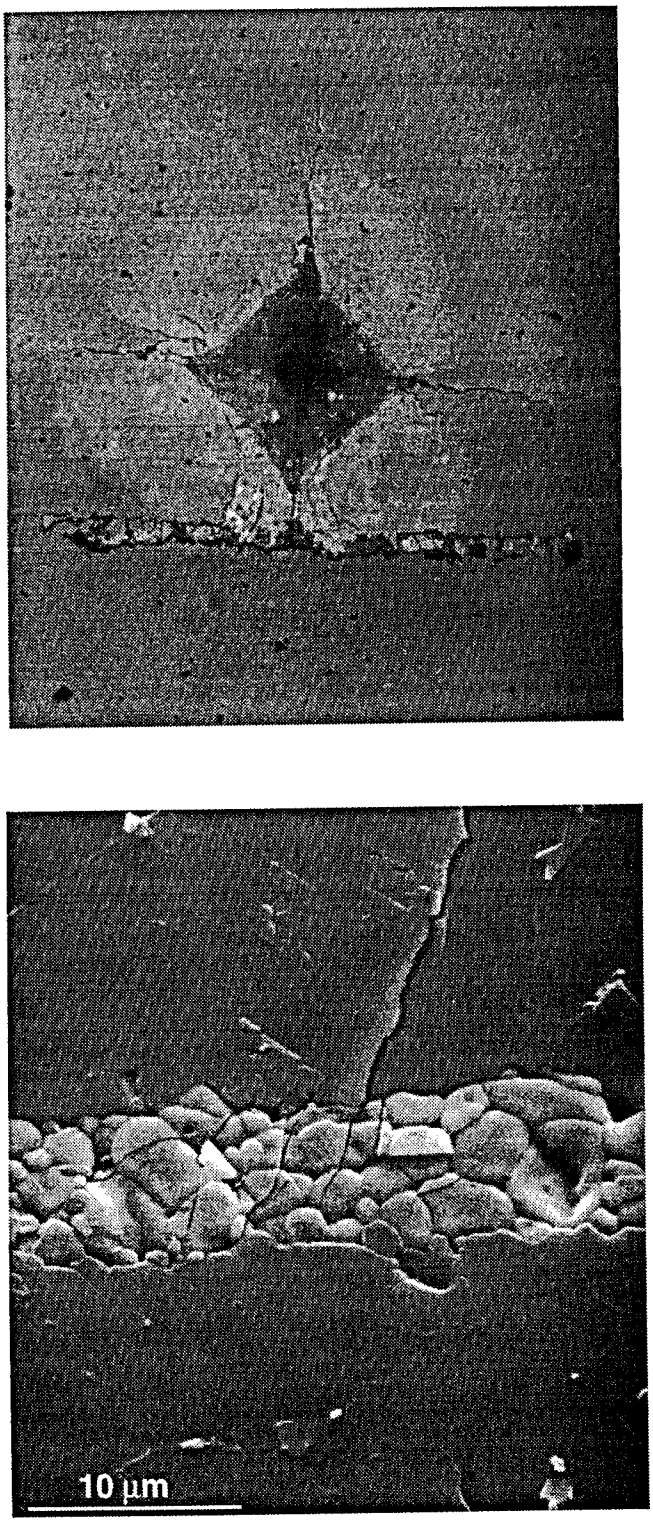

Fig. 4

(a)

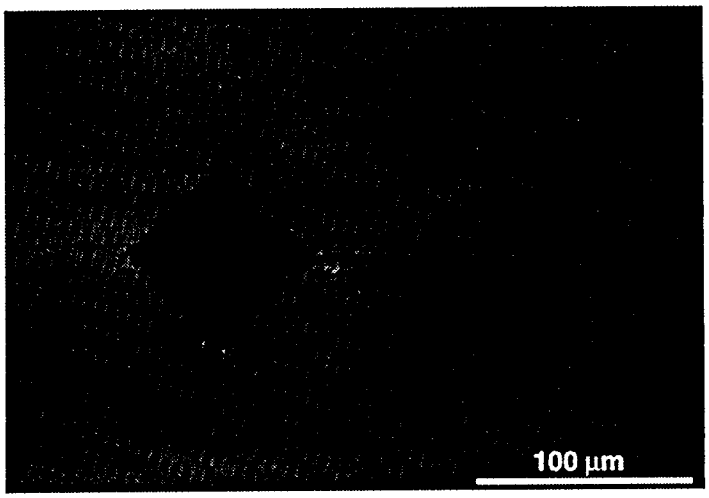

(b)

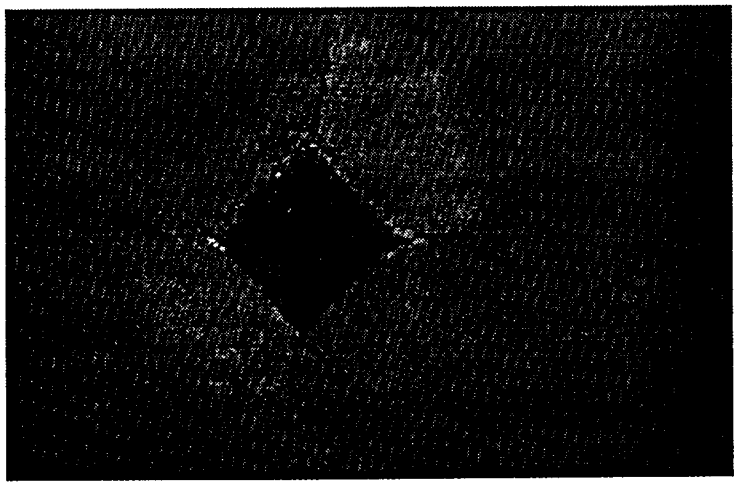

Fig. 5

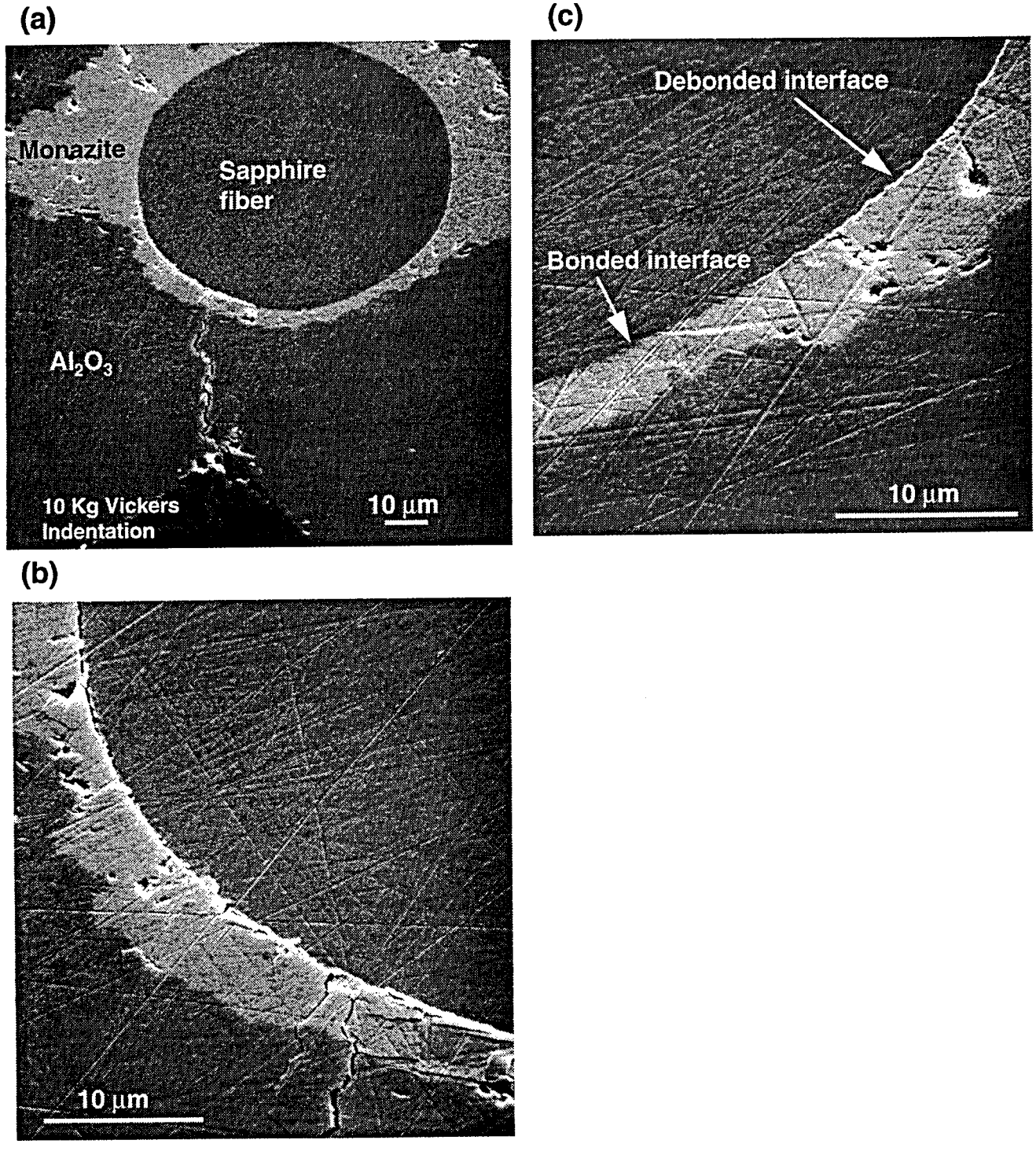
(a)
Monazite
Sapphire fiber
Al_2O_3
10 Kg Vickers Indentation
10 μm
(c)
Debonded interface
Bonded interface
10 μm
(b)
10 μm

Fig. 6

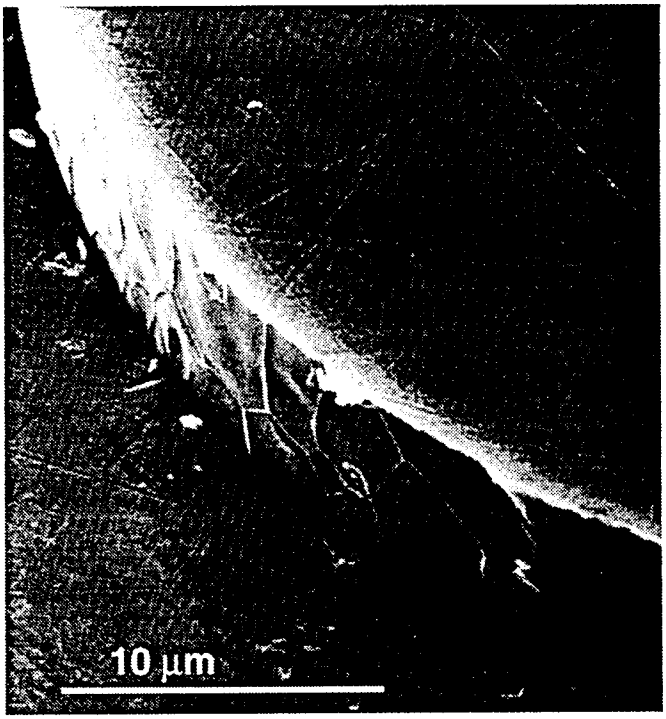

Fig. 7

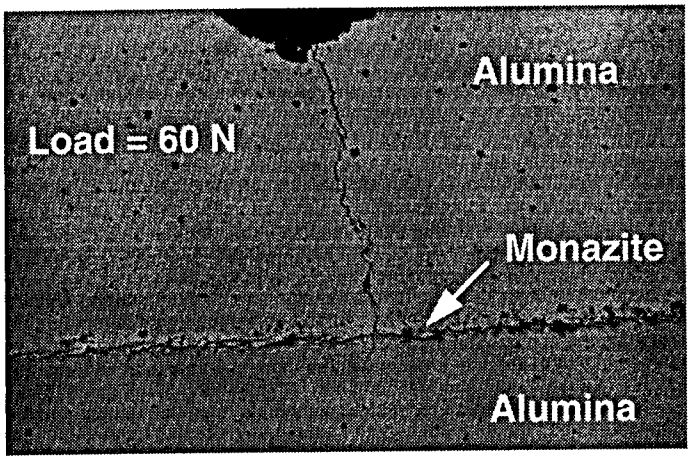

(a)

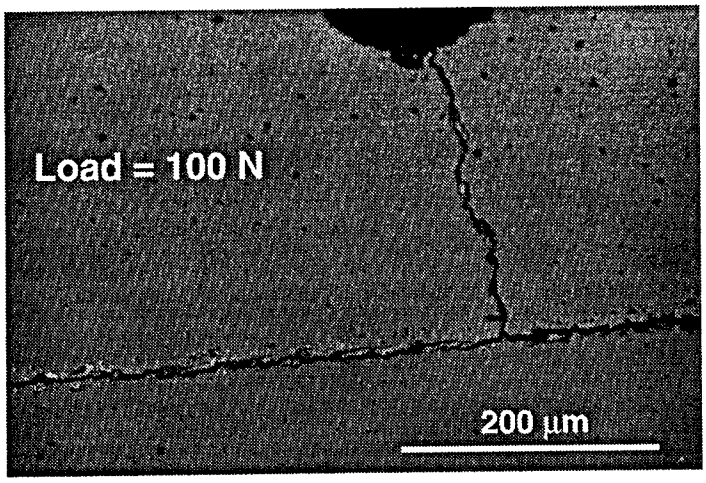

(b)

Fig. 8

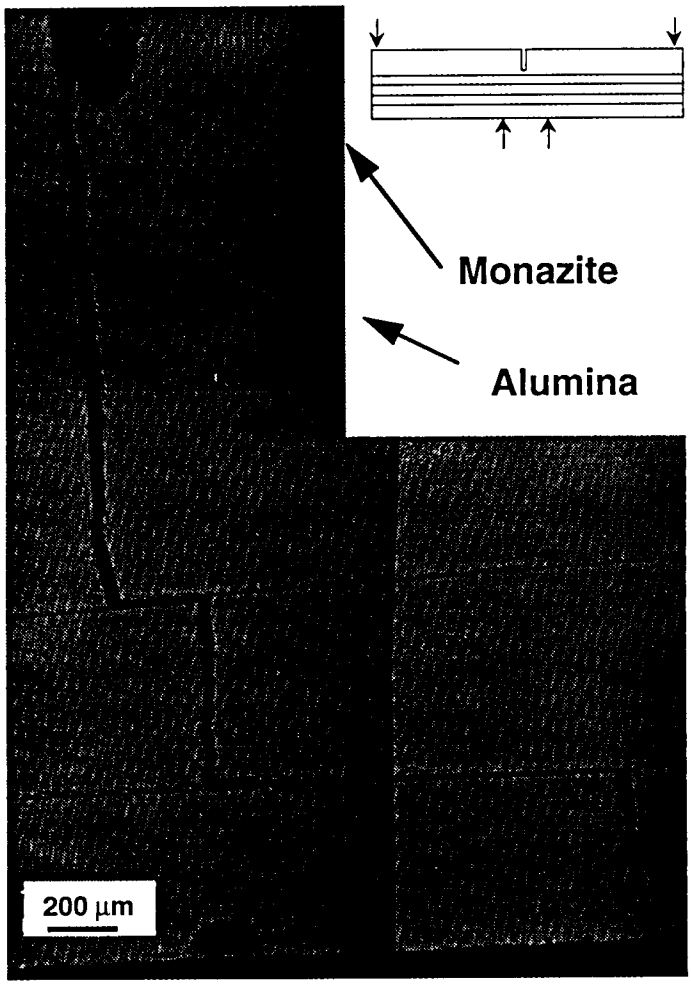

Fig. 8(c)

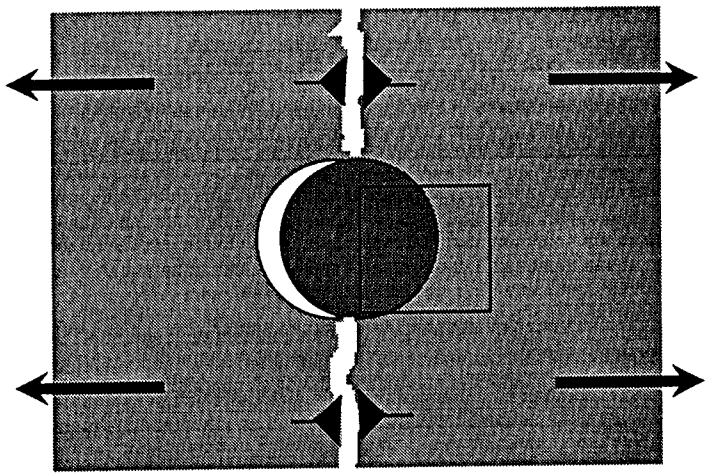

(a)

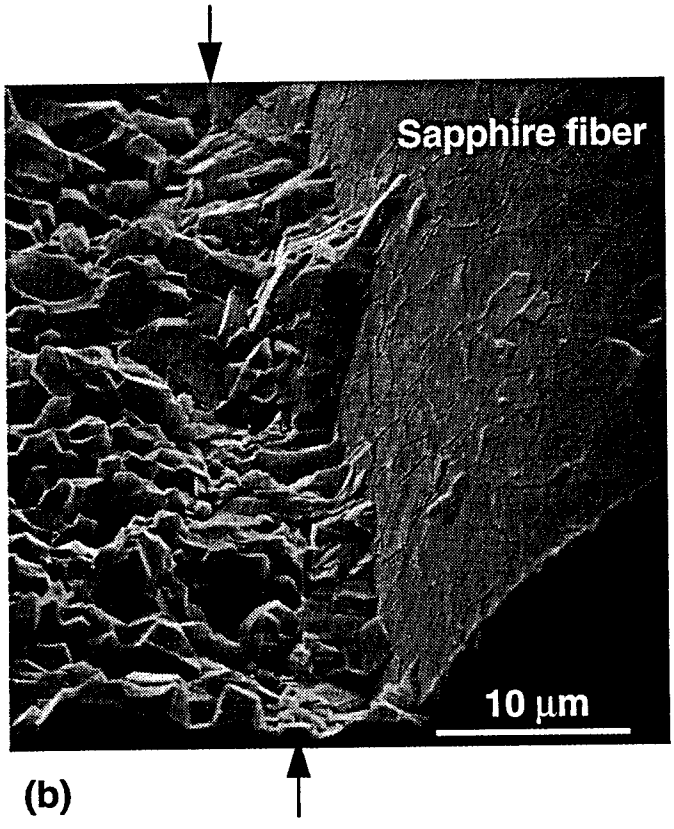

(b)

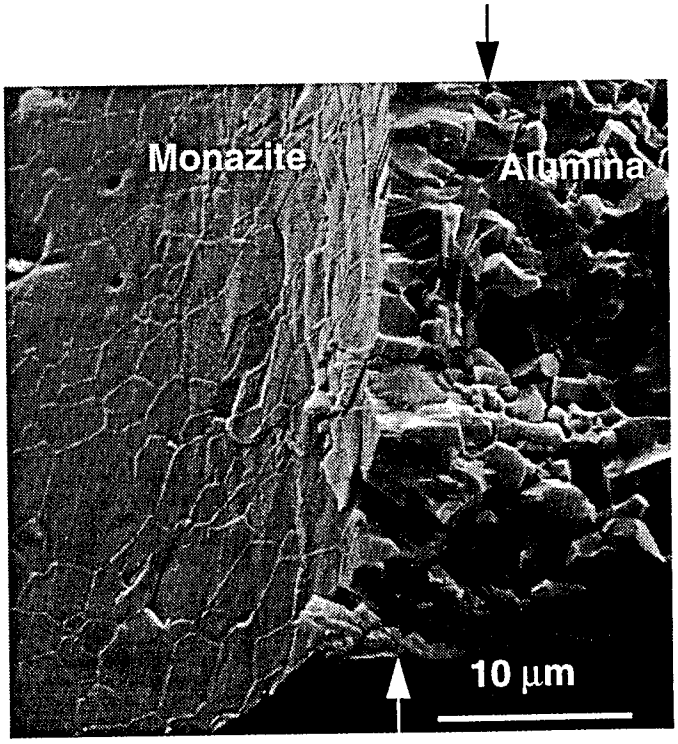

(c)

Fig. 13

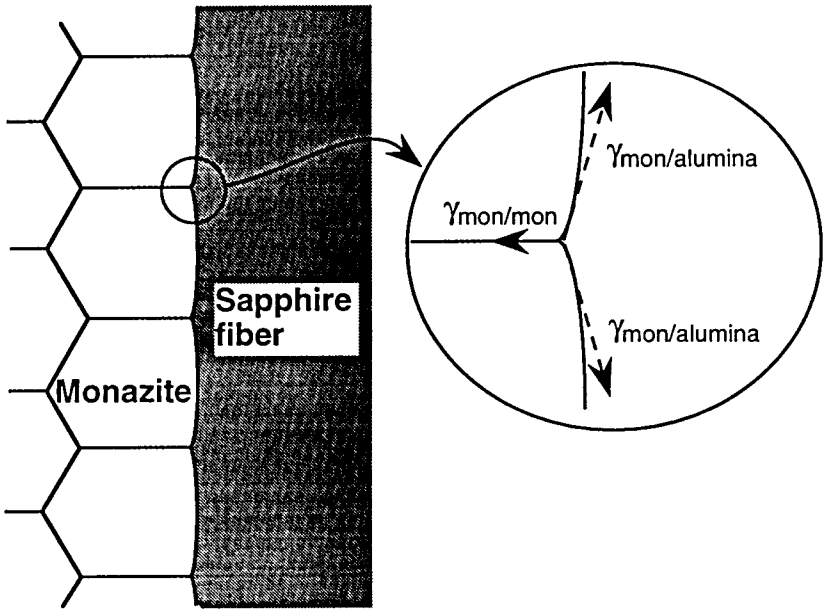
Sapphire fiber
Monazite
γmon/alumina
γmon/mon
γmon/alumina

Fig 13 (d)

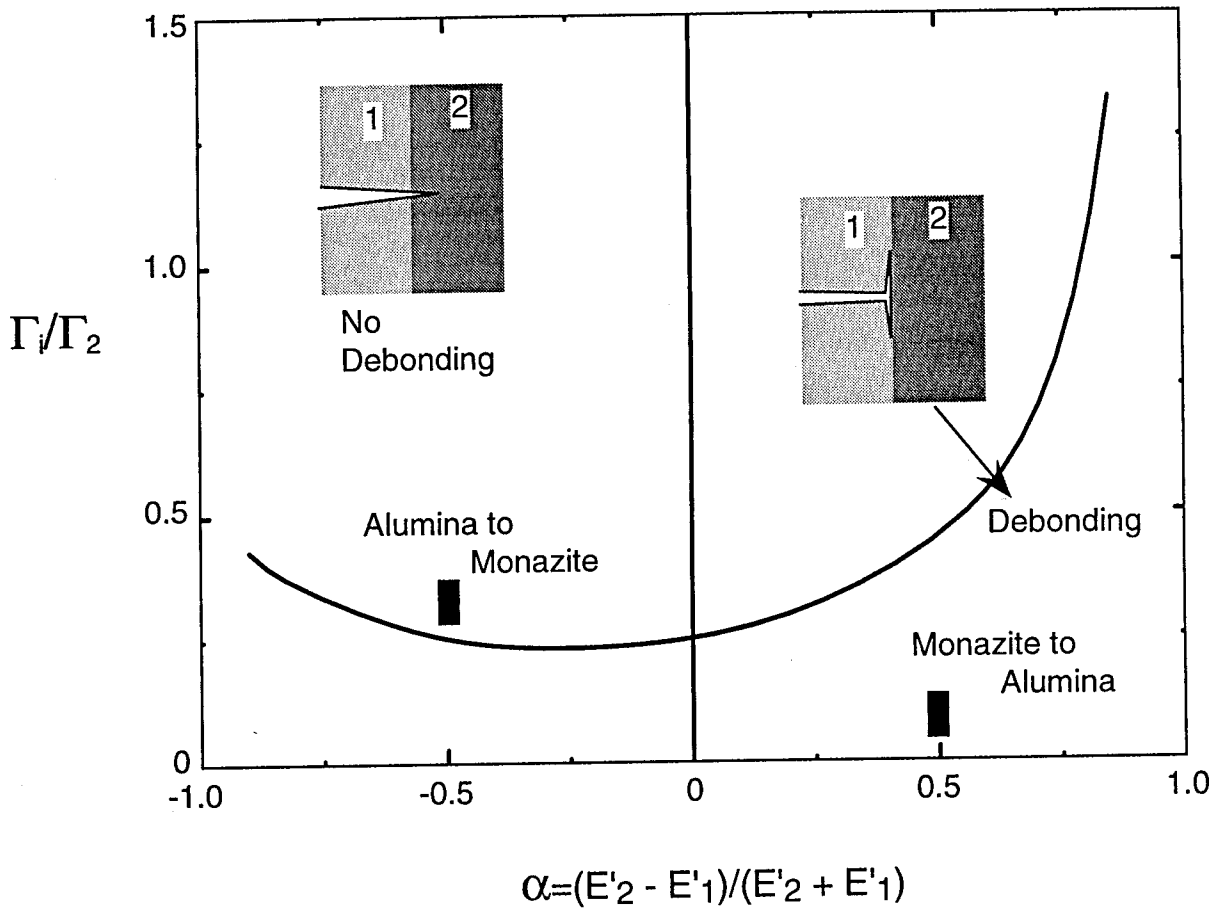
1.5
1.0
0.5
0
-1.0
-0.5
0
0.5
1.0
Γ_i/Γ_2
1
2
No
Debonding
1
2
Debonding
Alumina to
Monazite
Monazite to
Alumina
$\alpha=(E'_2 - E'_1)/(E'_2 + E'_1)$

FIG. 14

6.0 High Temperature Stability of Monazite–Alumina Composites

To be published in the *Journal of Materials Science and Engineering*

PP 94-124

Rockwell

Materials Science, Rockwell Science Center

HIGH TEMPERATURE STABILITY OF MONAZITE-ALUMINA COMPOSITES

Peter E. D. Morgan,
David B. Marshall, and
Robert M. Housley
Rockwell Science Center
1049 Camino Dos Rios
Thousand Oaks, CA 91360

Submitted to *J. Mat. Sci. Eng.*, July 1994

HIGH TEMPERATURE STABILITY OF MONAZITE-ALUMINA COMPOSITES

Peter E. D. Morgan, David B. Marshall and Robert M. Housley
Rockwell Science Center
1049 Camino Dos Rios
Thousand Oaks, CA 91360

ABSTRACT

The chemical and morphological stability and debonding characteristics of monazite-alumina interfaces are examined at temperatures of 1400°C and 1600°C. In the absence of impurities, the interface was stable for long periods (24h) at 1600°C and retained its ability to prevent crack growth by debonding. However, in the presence of alkali or divalent elements (K, Mg, Ca and others) at a free surface, La-containing β-alumina/magnetoplumbite platelets form near the interface. We propose that these elements stabilize the β-alumina/magnetoplumbite structure by tending to form the more stable "stuffed" structure closer to the magnetoplumbite type.

July 1994
for J. Mat. Sci. Eng.

1.0 INTRODUCTION

We recently found that $LaPO_4$ (La-monazite, hereinafter referred to simply as monazite) is a suitable interphase for ceramic composites containing alumina as both the matrix and the reinforcement [1]. The appeal of such composites is their high temperature oxidation resistance. The requirements for an interphase are compatibility (both chemical and morphological) with the matrix and reinforcement, stability in high temperature oxidizing environments, and weak bonding to allow crack arrest and toughening. In the previous study [1], the compatibility of Al_2O_3 and monazite was evident under both of the conditions used to fabricate the composites (hot pressing in graphite dies at 1400°C and sintering in air at 1600°C), while debonding at monazite-alumina interfaces in both fibrous and laminar composites was demonstrated using several mechanical tests.

The purpose of this paper is to examine in more detail the chemical compatibility and the morphological character of the alumina-monazite interface in the presence of low level impurities. In a closed system, monazite is believed to be phase compatible with alumina up to the eutectic melting point; by scanning electron microscopy we have detected no sign of eutectic melting up to 1750°C in air. Monazite itself melts at 2072°C without decomposition [2], whereas alumina melts at ~2030°C. In mineral assemblages the two commonly exist together, having crystallized from melts (e.g. [3]).

2.0 EXPERIMENTAL

Initially we used an "hydrated monazite" ($LaPO_4.\sim{}^1/_2H_2O$) from the Stremm chemical company, guaranteed at only 99% purity. It was determined that the material contained about 1% potassium owing to its method of preparation and so later work was

done using material that was washed several times in cold water, which lowered the potassium content to <0.3%. For good results the monazite was well mixed with 1wt% AlOOH (disperal®) and prefired to 1100°C to ensure that the monazite was solid solution saturated with alumina. At this level, alumina is always found in the product, confirming that the solid solution limit, which is immeasurably low by XRD lattice parameter measurements (but not likely zero), has been exceeded. After this treatment the powder was milled (with high purity alumina balls) and sieved to <325 mesh. Slurries for coating alumina fibers or plates, etc., were readily made by shaking this powder with isobutanol. In more recent work we are synthesizing** a hexagonal rhabdophane structured $LaPO_4.\sim{}^1/_2H_2O$ precursor to monazite, which it was confirmed again, gave better results after preheating to 1100°C with well mixed 1wt% AlOOH.

Several types of fibrous and laminar composites were assessed. Initially a composite consisting of sapphire fibers in a monazite matrix was fabricated by embedding sapphire fibers (Saphikon Company) in the unwashed monazite and hot pressing at 1200°C. A second fibrous composite was fabricated by coating the sapphire fibers with a monazite slurry as already described, embedding the fibers in alumina powder matrix (Ceralox) containing 0.5% by weight of MgO as a sintering aid, and hot pressing at 1400°C. Finally, multilayered composites of alumina and monazite were fabricated by first forming a layered green body colloidally by sequentially vacuum slip casting layers of monazite (washed and prefired) and high purity alumina (Sumitomo 99.99% α-Al_2O_3), and then packing the green body in dry alumina and hot pressing at 1400°C. (Layered composites have also been densified by sintering in air at 1600°C [1].)

** to be published in more detail later.

The composites were sectioned and polished to allow observation of microstructural changes during subsequent heat treatment. The ability of the monazite-alumina interfaces to debond was tested using indentation cracks as described elsewhere [1]. A beam of the alumina-matrix composite containing coated fibers, with a polished surface normal to the fibers, was repeatedly heat treated in air under the following conditions: 0.5h at 1400°C; 10h at 1400°C; 2h at 1600°C; and 24h at 1600°C. After each heat treatment, a Vickers indenter was loaded in the matrix near a fiber, oriented so that a crack from the indentation would intersect the fiber.

3.0 RESULTS AND DISCUSSION

3.1 Interfacial Debonding

The heat treatments at 1400°C and 1600°C did not change the mechanical response of the monazite-alumina interface. In all cases the indentation cracks passed from the polycrystalline alumina matrix into the monazite coating but did not cross from the monazite coating into the alumina fiber. Instead, the crack deflected around the fiber, which debonded cleanly at the interface (Figs. 1 and 2(c)). Usually several cracks formed in the monazite coating. The response is consistent with the analysis of interfacial debonding of He and Hutchinson [4] and the measured fracture energies of alumina, monazite and the alumina-monazite interface [1].

3.2 Microstructure and Chemistry

In accordance with the aforesaid compatibility of monazite and alumina, in the interior of the specimens, whether layered laminates of alumina and monazite or single crystal alumina fibers contacting monazite, no reaction was seen upon hot pressing at 1400°C in N_2 or sintering at 1600°C in air [1]. Further heat treatments at 1400°C and 1600°C in air engendered only minor grain growth in the monazite and polycrystalline

alumina, without altering the morphology of the interfaces between the monazite and alumina. The details of grain growth on an exposed polished surface can be seen in Fig. 2, which shows the surface of the coated sapphire fiber composite after each of the treatments mentioned previously.

On exposed surfaces such as in Fig. 2, reactions have been observed after heat treatment at 1600°C, resulting in formation of hexagonal β-alumina/magnetoplumbite (BAMP) platelets (often with clearly visible 120° prism faces) near the alumina-monazite interfaces (Figs. 2(c) and 3). The phases are shown clearly in the back scattered electron image of Fig. 3(b): the darkest phase is alumina; the lightest phase surrounding the sapphire fiber is the monazite (with 1% alumina); while the lighter gray platelets on the fiber and within the polycrystalline alumina matrix beyond the monazite are the lanthanum-containing BAMP. All identifications were checked with EDS. Later serial polishing of the surface shown in Fig. 2(c) showed that the reaction is confined to the near-surface region: the concentration of BAMP platelets decreased rapidly below the surface (Fig. 2(d)) with no platelets being observed at depths greater than ~50 μm. We may immediately conclude that either material has been lost from the surface (e.g., phosphate) or pickup of reactive impurities from the atmosphere in the furnace occurred, or both possibilities together.

EDS of the BAMP platelets indicated low levels (a few %) of Mg and K, unsurprising as the monazite used at this time had low levels of K and the matrix alumina contained 0.5% Mg added as a sintering aid (magnesia is quite volatile at 1600°C). A few percent of Ca was also present, which we believe came from the furnace atmosphere (as we frequently use calcium oxide in the furnaces to getter silicon and molybdenum

which sometimes emanate from the $MoSi_2$ heating elements).[+] These elements probably stabilize BAMP by tending to form the more stable, "stuffed", more nearly MP type [5]. BAMP here ranges between possible end-member types "$LaAl_{11}O_{18}$"*, $K_{1/2}La_{1/2}Al_{12}O_{19}$, $CaAl_{12}O_{19}$, and $LaM^{2+}Al_{11}O_{19}$ [5]. This latter compound is of the true magnetoplumbite (MP) variety, with $La^{3+}M^{2+}$being a valence coupled substitution for $Ca^{2+}Al^{3+}$ in the prototypical $CaAl_{12}O_{19}$, hibonite, parent. No other commonplace impurities, such as silicon or iron, were detected.

A surprising discovery was next encountered when the samples were refired in air (for 2 hours) at 1400°C, whereupon the BAMP disappeared to be replaced at each site by monazite and leaving "ghost impressions" of BAMP, Figs. 3(c) and 3(d). This raises questions about the lower temperature stability of the particular form of BAMP present. Unfortunately, we have found no good literature data on the lower temperature stability of the more β-type "$LaAl_{11}O_{18}$", although it is known that $LaM^{2+}Al_{11}O_{19}$,which is believed to be more stable, forms by 1200°C [5] on heating precursors. Supporting experiments on this are underway. Even if the BAMP were nominally stable in air at 1400°C, it is possible that excess phosphate is available in this environment allowing the reconversion to monazite. Initial firings to 1400°C, as would be expected by the above discussion, do not produce any BAMP.

The formation of BAMP was much more sluggish in the multilayered alumina-monazite composite that was fabricated using high purity alumina powder (without MgO sintering aid). After 2 hours at 1600°C there were no BAMP platelets evident on the surface (Fig. 4). Only after 24 hours at 1600°C were small numbers of platelets observed

---

[+] The effects of impurity pickup from furnaces become rather apparent when very small scale model experiments are being conducted, so that resort to getters and buffer powders is very necessary.

* in quotes as the composition is somewhat indefinite.

in localized regions of the alumina layers (Fig. 5); the amount of BAMP here was much less than in the Mg-containing alumina of Figs. 2 and 3 after only 2 hours heat treatment. Low levels of Ca but no Mg were detected by EDS in this BAMP. Because the alumina in the layered composite does not contain Mg, the alumina grain size is much larger than in the fibrous composite of Figs. 1 and 2. However, the microstructure is remarkably stable; the morphology of the layers and the grain size of the Al_2O_3 and monazite did not change significantly after 24 hours at 1600°C (Fig. 5).

In a particular instance, sieving of the monazite had been done aggressively using an automatic sieve shaker, whereupon the monazite evidently became contaminated, changing color from white to light gray and then to a light beige on firing. The material *always* showed BAMP on firing with alumina. EDS analysis of this revealed, in addition to the K (now lowered to about 1%) and Ca, a few percent of Cu and Zn which had been picked up from the sieves, again stabilizing BAMP by forming solid solutions with the more stable $LaM^{2+}Al_{11}O_{19}$ type ($M^{2+} = Cu^{2+}$, Zn^{2+}in this case). Because the BAMP itself was formed only at a low level, the Cu^{2+} and Zn^{2+}were scavenged to much more concentrated levels in the BAMP than was seen to exist in the monazite. In this way the BAMP becomes a useful *solid state indicator* of the existence of some particular impurities.

3.3 Interface Morphology

Monazite-sapphire interfaces that were separated by fracture in three different composites are shown in Figs. 6 to 8. In all cases the separation occurred exactly along the interface, revealing the details of the interface morphology. The composite with sapphire fibers in the K-containing monazite matrix, which was hot pressed at 1200°C, is shown in Fig. 6. Some large pores in the matrix are evident in Fig. 6(a), as are remnants of a potassium-aluminum-phosphate liquid phase at the hot pressing temperature [1]. The

faceted grooves and ridges on the surface of the fiber (and replicated in the separated matrix) are very similar to surface features reported by Davis et al. after heat treating bare sapphire fibers in air [6]. A small reduction in fiber strength (~10%) was observed in that study after heat treatment at 1250°C, although this was associated with damage from local chemical reactions rather than the grooves. However, if they were allowed to coarsen, such faceted grooves would be expected to degrade the strength.

A different morphology was observed in composites that were hot pressed at higher temperatures (Figs. 7 and 8). Here ridges formed on the sapphire fiber surface where the monazite grain boundaries intersected the fiber, while the surface between the ridges is smoothly curved. The smooth curvature indicates that there are no preferred low energy orientations for the monazite-alumina interface (which is an advantage for an interface that is required to debond, since low energy interface regions would be more strongly bonded). The geometry of the ridges (i.e., the dihedral angle at the intersection of the monazite grain boundary and the monazite-alumina interface) is dictated by the grain boundary and surface energies [1]. However, the reason for the more pronounced ridges in Fig. 8 is not clear. The fiber in Fig. 8 was embedded in a thick monazite layer in the multilayered composite that was consolidated colloidally and hot pressed for 2h at 1400°C, whereas the fiber in Fig. 7 is from the composite containing coated fibers in an alumina matrix, which was hot pressed for 1h at 1400°C. However, it was not simply the longer time at high temperature that caused the more pronounced ridges; other specimens of the composite in Fig. 7 were subsequently heat treated for longer periods at both 1400°C and 1600°C without changing the interface morphology (see Fig. 2(c)).

The ridges in Figs. 7 and 8 are not expected to degrade the fiber strength significantly [1]. Indeed, these results suggest that a fully dense monazite coating on a sapphire fiber may play a protective role in stabilizing the fiber surface against the potentially detrimental faceting that occurs on an exposed sapphire surface at high

temperature. Thus, interestingly, the strength of the fibers in a composite could be higher than the strength of equivalently heat treated bare fibers.

4.0 CONCLUSIONS

Low level surface (not bulk) reaction between monazite and alumina at 1600°C, to produce β-alumina/magnetoplumbite (BAMP) products, is suggested to be allowed by loss of phosphorus and also encouraged by the presence of monovalent and divalent impurities which are highly scavenged by the BAMP phase. BAMP is highly refractory, unlike the detrimental phases produced by impurities in many other systems. The need for extremely detailed study is suggested; and toward that end we are making a large-scale, standard, highly pure grade of monazite for model studies of coated fibers.

In the bulk the monazite-alumina interface was stable (both chemically and morphologically) and retained its ability to debond after heating in air for 24h at 1600°C.

ACKNOWLEDGEMENTS

Funding for this work was provided by the U.S. Office of Naval Research (Dr. S. Fishman) under Contract N00014-91-C-0157. The authors are grateful to Mr. E. Wright for assistance with specimen preparation.

REFERENCES

1. P.E.D. Morgan and D.B. Marshall, Composites of Monazite and Alumina for High Temperature Oxidizing Environments, submitted to *J. Am. Ceram. Soc.*

2. Y. Hikichi and T. Nomura, Melting Temperatures of Monazite and Xenotime, *J. Am. Ceram. Soc.* **70** (1987) C252-3.

3. M.L. Dele, P. Dhamelincourt and H.J. Schubnel, Application of a Raman Laser Microprobe for Determining Inclusions in Various Gems, *Samotsvety. Mater. S'ezda NMA*, Ed. A. V. Sidorenko (1980) pp 5-17.

4. M.-Y. He and J.W. Hutchinson, Crack Deflection at an Interface Between Dissimilar Materials, *Int. J. Solids Struct.* **25** (1989) 1053-67.

5. P.E.D. Morgan and J.A. Miles, Magnetoplumbite-Type Compounds: Further Discussion, *J. Am. Ceram. Soc.* **69** (1986) C157.

6. J.B. Davis, J. Yang and A.G. Evans, Effects of Composite Processing on the Strength of Sapphire Fiber Reinforced Composites, *Acta Metall. Mater.*, in press.

Figure Captions

1. Scanning electron micrographs showing interaction of indentation crack with monazite-coated sapphire fiber.

2. Scanning electron micrographs showing microstructural changes in an area of a composite (polycrystalline alumina matrix with monazite-coated fibers) after repeated heat treatments.

   (a) polished surface after 1h at 1400°C in air.

   (b) same surface after a further 10h at 1400°C in air.

   (c) same surface after a further 2h at 1600°C in air. After this heat treatment a Vickers indenter was loaded on the matrix as in Fig. 1 causing the cracking visible to the right of the micrograph. Note that the cracks arrest at the interface between the monazite and the sapphire fiber.

   (d) same area as (c) after polishing to a depth of ~20 μm, showing smooth fiber-monazite interface. Holes in the monazite coating were caused by chipping of the indentation induced cracks visible in (c) during polishing.

3. (a) Secondary electron image of alumina/monazite-coated-sapphire composite after heat treatment at 1600°C for 2h in air showing β-alumina/magnetoplumbite platelets.

(b) Backscattered electron image of (a): lightest areas are monazite; darkest regions are alumina; and gray regions are β-alumina/magnetoplumbite.

(c) Same area as (a) after further heat treatment at 1400°C for 2h.

(d) Backscattered electron image of (c).

4. Laminar monazite-alumina composite after 2h at 1600°C in air.

5. Laminar monazite-alumina composite after 24h at 1600°C in air.

6. (a) and (b) matching fracture surfaces of fiber-matrix interface in monazite-matrix composite.

7. (a) and (b) matching fracture surfaces from sapphire fiber-monazite interface in composite containing coated sapphire fibers. Arrows indicate boundary between monazite coating and polycrystalline Al_2O_3 matrix.

8. (a) and (b) matching fracture surfaces from sapphire fiber-monazite interface in laminar alumina-monazite composite containing sapphire fibers in a monazite layer.

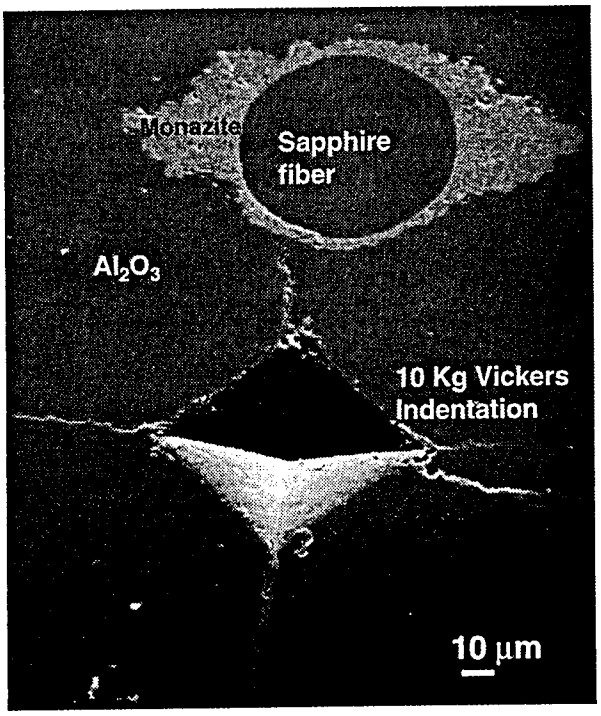
Monazite
Sapphire fiber
Al_2O_3
10 Kg Vickers Indentation
10 μm

(a)

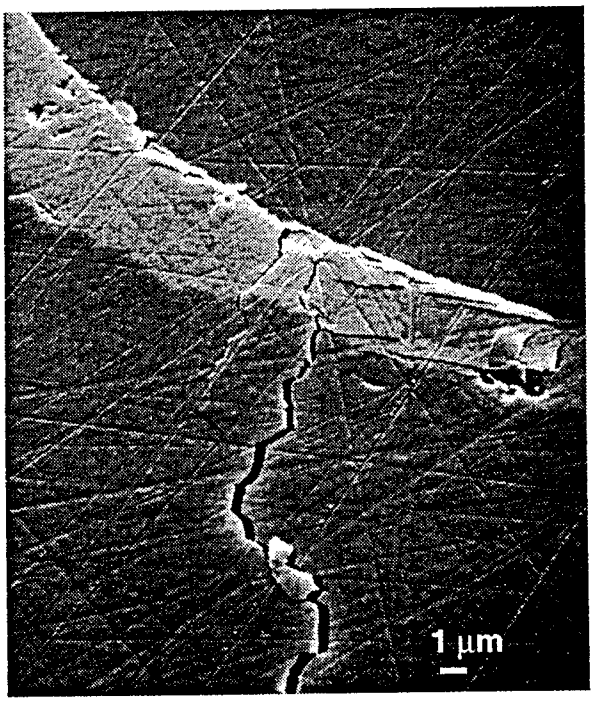
1 μm

(b)

Fig. 1

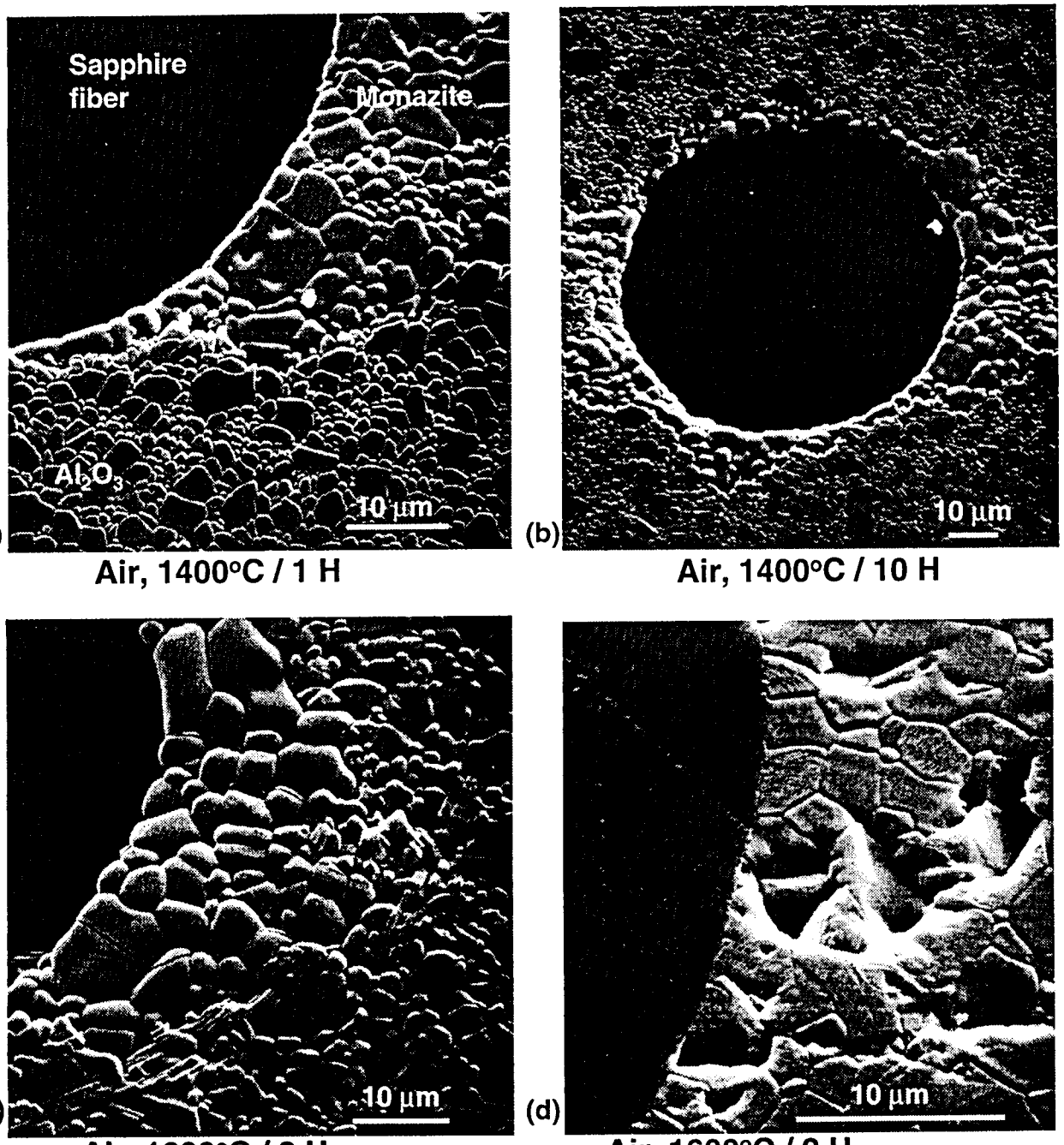
Sapphire fiber
Monazite
Al_2O_3
10 μm
(a)
Air, 1400°C / 1 H
10 μm
(b)
Air, 1400°C / 10 H
10 μm
(c)
Air, 1600°C / 2 H
10 μm
(d)
Air, 1600°C / 2 H
20 μm polished from surface

Fig. 2

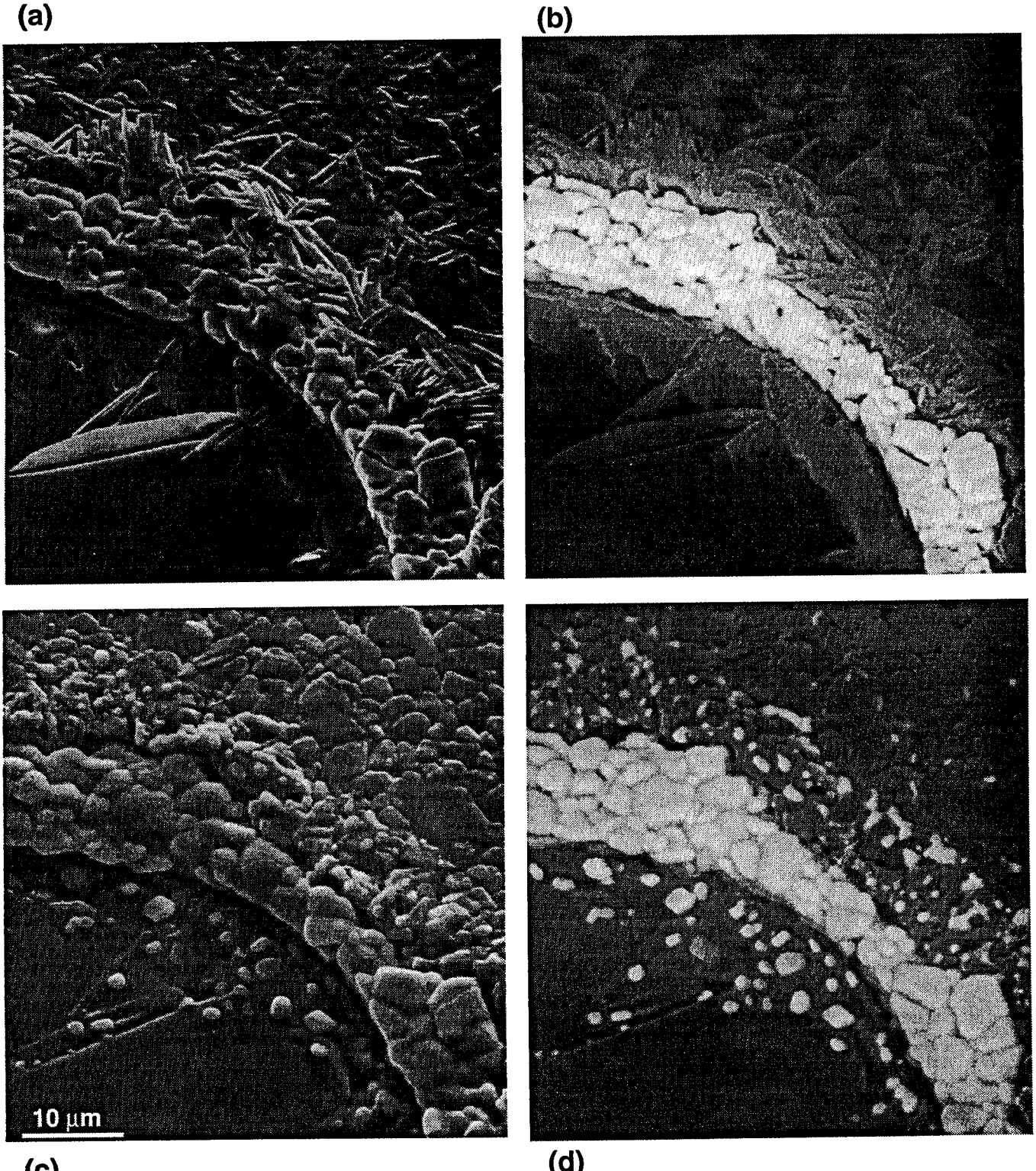

Fig. 3

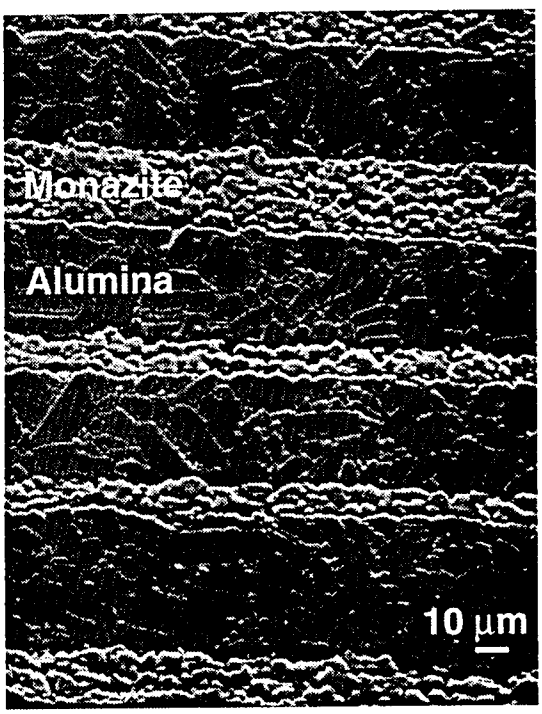

(a)

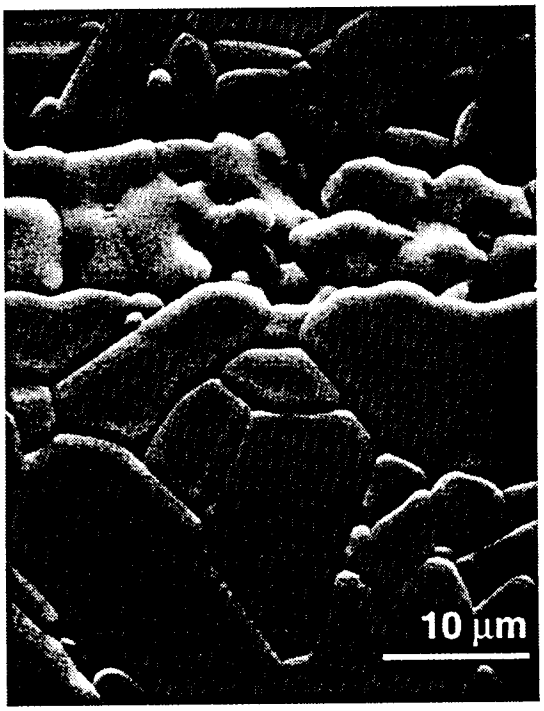

(b)

Fig. 4

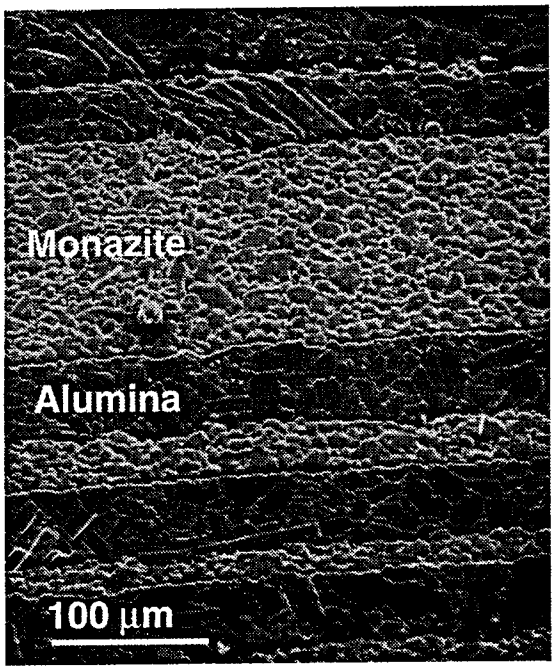

(a)

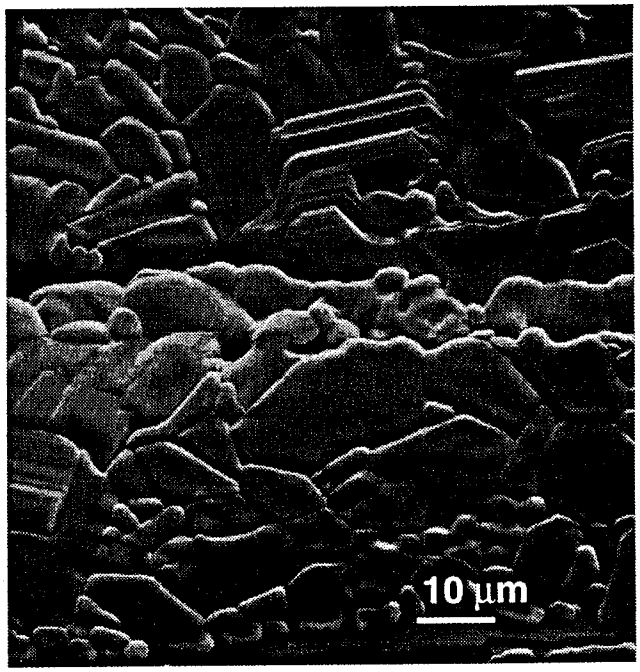

(b)

Fig. 5

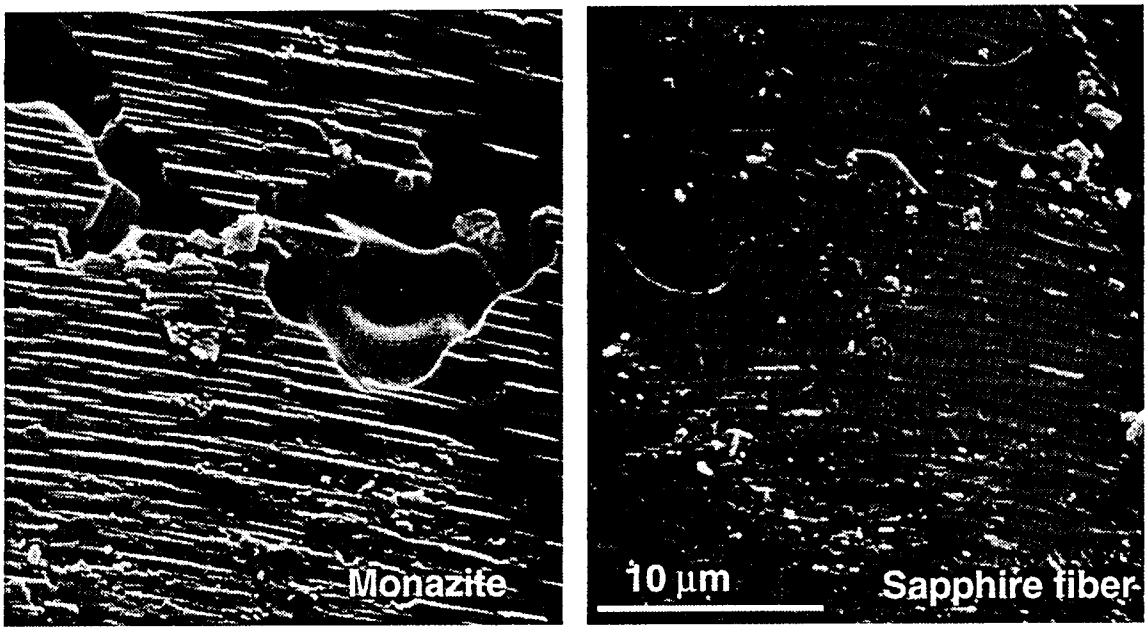

(a)

(b)

Fig. 6

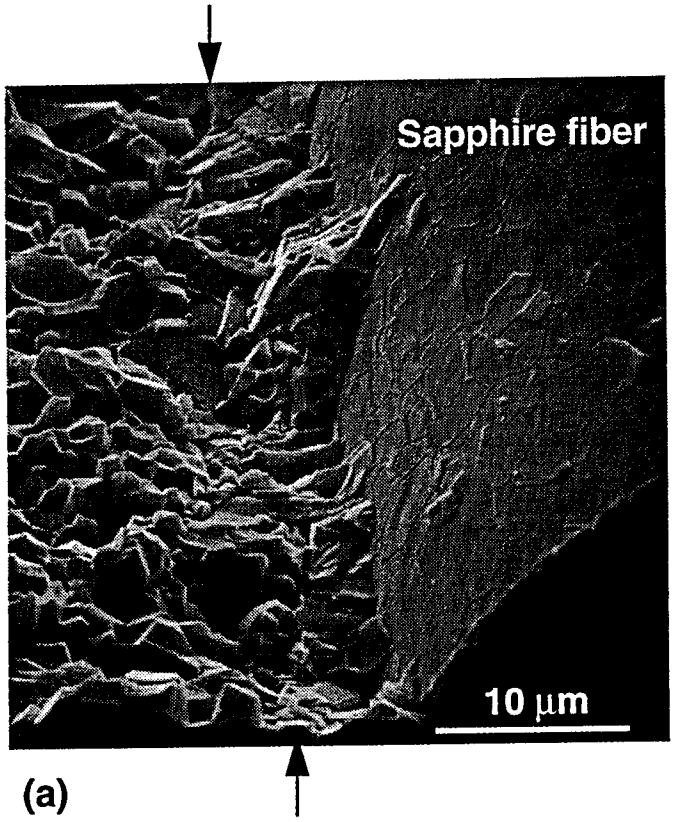

(a)

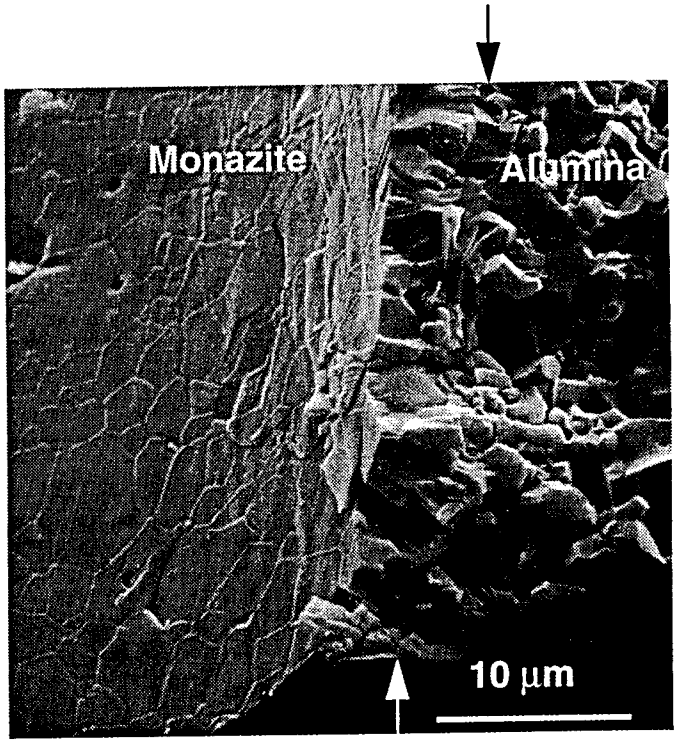

(b)

Fig. 7

M2/1 030194-1,2

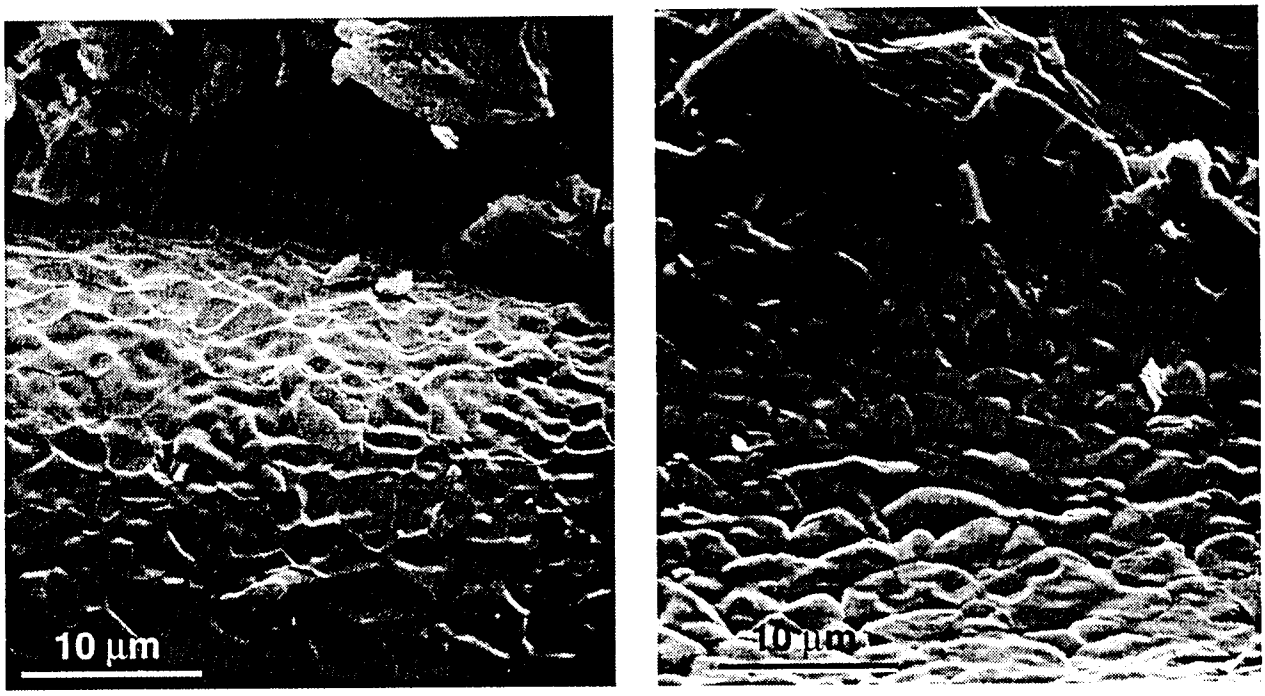

Fig. 8